8-2018

Experimental Comparison Between Hollow Cathodes with Cermet, Lanthanum Hexaboride, and Barium Oxide Insert Materials

Nagual Simmons
Western Michigan University, nasimmons87@gmail.com

EXPERIMENTAL COMPARISON BETWEEN HOLLOW CATHODES WITH CERMET, LANTHANUM HEXABORIDE, AND BARIUM OXIDE INSERT MATERIALS

by

Nagual Simmons

A thesis submitted to the Graduate College
in partial fulfillment of the requirements
for the degree of Masters of Science
Mechanical Engineering
Western Michigan University
August 2018

Thesis Committee:

Dr. Kristina Lemmer, Ph.D., Chair
Dr. Jennifer Hudson, Ph.D.
Dr. Mike McDonald, Ph.D.

EXPERIMENTAL COMPARISON BETWEEN HOLLOW CATHODES WITH CERMET, LANTHANUM HEXABORIDE, AND BARIUM OXIDE INSERT MATERIALS

Nagual Simmons, M.S.

Western Michigan University, 2018

This thesis compares two different hollow cathode assemblies (HCA) using three different insert materials. NASA's Jet Propulsion Laboratory (JPL) provided the H6 HCA and the Lanthanum Hexaboride (LaB_6) insert. A barium oxide (BaO) insert was purchased from E-beam and used with the H6 HCA. The novel Cermet material was purchased from Plasma Controls, LLC and the HCA was based on the JPL H6 HCA. Plasma properties in the external region of all three inserts and the internal region of the LaB_6 were determine using two separate Langmuir probes. Various operating points were tested at a combination of flow rates and keeper and discharge currents. The ion number densities of both the LaB_6 and BaO were compared with those measured in the plume of the Cermet cathode. It was determined that the Cermet produced higher ion number densities than the similarly sized LaB_6, but only produced similar ion number densities between 25 – 40 mm downstream of the orifice plate for the BaO insert. Using the cathode internal probing box internal and external plasma properties of the LaB_6 was analyzed. The trend of the ion density showed good agreement with literature. Telemetry data at stable operating points are presented.

ACKNOWLEDGMENTS

I would like to thank my advisor, Dr. Kristina Lemmer for providing me guidance and support when I needed it. You have shown me that working on space technology is something that is not out of my reach. You have always led by example and to me, have set a standard as a researcher, instructor, and role model.

I'd like to thank Matthew Baird, a fellow student, lab partner, and good friend. We spent countless hours talking about electric propulsion diagnostics and designs. You always made yourself available if I needed to bounce ideas off of you and help me if I was in a fog.

I would also like to thank the other students that worked in the lab: Margaret Mooney, Thomas Kerber, Sarah Sokolski, and Hannah Watts, as well as the postdoc Nick Taylor. Together you guys gave the lab an atmosphere that was built around learning and helping one another.

Lastly, I would like to thank my wife, Angela Simmons. Regardless of the long hours I put in for school, you focused on the time we spent together. I could not have done it without you.

Nagual Simmons

Table of Contents

1 Introduction 1

1.1 Background 1

1.2 Research Motivation 5

1.3 Organization 7

2 Background 8

2.1 Milestones in Cathode Development 8

2.2 Insert Development 10

2.3 Alternative Insert Materials 11

3 Experimental Setup and Methodology 14

3.1 Langmuir Probe Theory 14

3.2 Facilities 16

3.3 Hollow Cathodes Assemblies 17

3.4 Methodology 18

3.4.1 Overview 18

3.4.2 Experimental Setup 19

3.4.3 Telemetry Data 22

3.4.4 Langmuir Probe Data 24

Table of Contents - Continued

4 Results and Discussion 26

4.1 Ignition 26

4.1.1 LaB_6 26

4.1.2 BaO 26

4.1.3 Cermet 28

4.2 External Probing Results 29

4.2.1 Telemetry 30

4.2.2 Plasma Properties 33

4.3 Internal Probing Results 40

5 Conclusions and Remarks 43

5.1 Future Work 44

References 46

Appendix A 49

Appendix B 59

List of Figures

1 - Schematic of a hollow cathode assembly with labelled components [1]. 3

2 - Three orifice plate aspect ratio configurations [1]..... 4

3 - Electron current density as a function of temperature for various insert materials [1]. 5

4 - Early construction of cathodes: Left) Brush type; Middle) Independent heated cathode; Right) Oxide-magazine cathode [14]..... 8

5 - Early constuction of hollow cathodes with labelled components [16]. 9

6 - Keeper voltage vs flow rate curve for starting the Cermet HCA. 13

7 - I-V curve taken with a LP..... 15

8 - HCAs used in the experiment. Left) Plasma Controls Right) JPL 17

9 - Schematic of Plasma Controls H6-type HCA 18

10 -Internal probe box without the cathode, seal, and plexiglass top. 20

11 - Electrical configuration of HCA setup. 21

12 – Experimental layout inside vacuum chamber. 22

13 - RGA100 monitoring results during conditioning process of the BaO insert within the HCA..... 27

14 - Emission current of the BaO cathode recorded while heating the insert after conditioning. 28

List of Figures - continued

15 - BaO IVm map at an discharge current of 4 A. Red dots depict where telemetry was taken. 30

16 - LaB_6 IVm map at an discharge current of 4 A. Red dots depict where telemetry was taken. 31

17 - Cermet IVm map at an discharge current of 4 A. Red dots depict where telemetry was taken. 31

18 - Total power vs total current for the LaB_6 insert. Single data points that had multiple total currents and used 1.5 A for the keeper is represented by a square data point. 32

19 - Total power vs total current for the BaO insert. Single data points that had multiple total currents and used 1.5 A for the keeper is represented by a square data point. 33

20 - Total power vs total current for the Cermet insert. Single data points that had multiple total currents and used 1.5 A for the keeper is represented by a square data point. 33

21 - LaB_6 plasma properties for different flow rates, keeper, and discharge levels. kpr = keeper; An = anode 34

22 - BaO plasma properties for different flow rates, keeper, and discharge levels. kpr = keeper; An = anode 36

23 - Cermet plasma properties for different flow rates, keeper, and discharge levels. kpr = keeper; An = anode 38

24 – Normalized ion number density of (LaB_6/Cermet) vs downstream position for various flow rates. kpr = keeper; An = anode 39

25 - Normalized electron number density of (BaO/Cermet) vs downstream position for various flow rates. kpr = keeper; An = anode 40

List of Figures - continued

26 - Electron temperature as a function of position inside/outside the LaB_6 HCA. 41

27 - Plasma potential as a funcition of poition inside/outside the LaB_6 HCA..... 42

28 - Combined internal and external ion current density as a function of position inside/outside the LaB_6 HCA. 42

List of Tables

1 - Various work function for different materials. 5

2 - Geometrical ratios of the HCA 18

3 - Cathode placement inside vacuum chamber. 22

4 - Operating points tested for each HCA. 24

5 - Stable operating points marked with “X.” Shaded box is where LP data were collected. 29

6 - LaB_6 telemetry data 49

7 - BaO telemetry data 50

8 - Cermet telemetry data 51

1 Introduction

1.1 Background

Electric propulsion (EP) has gained popularity as a source of space propulsion because of the possible propellant mass savings it provides over conventional chemical propulsion systems. Unlike chemical rockets which have limitations set by the energy stored in chemical bonds, the energy input into EP rockets is only limited by the power source on-board the spacecraft. The energy is used to ionize neutral propellant and accelerate ions to generate thrust. Propulsion devices are often compared with each other by specific impulse (Isp); Isp is a measure of the total impulse that can be achieved per kg of propellant. Chemical propulsion is limited to an Isp of 450 s due to the energy stored in the chemical bonds, whereas the Isp in EP thrusters ranges from 300 s to 3600 s [1]. This high Isp makes EP thrusters an attractive option for deep space missions. The NASA technology roadmap has identified specific electric propulsion technologies as the primary thrusters for deep space missions [2].

Considered to be the fathers of rocketry, Oberth, Tsiolkovsky, and Goddard helped paved the way for today's advancements and research in electric propulsion. Tsiolkovsky derived the rocket equation,

$$T = M\frac{dv}{dt} \qquad \text{Eq. 1}$$

where T is thrust, M is mass of the spaceship, and v is velocity [1]. As propellant is used it changes the mass of the spacecraft. Therefore, long duration missions may need to consider the rate of change of the spacecrafts mass. This equation is used to compare different propellants for missions. Goddard developed and patented the first device that could ionize inert gases. Oberth

showed how EP could and must be used for space exploration [3]. After more than a decade of being forgotten, Shepard and Clever reexamined EP as a viable option for space propulsion. However, they concluded, that the power required to achieve the acceleration needed for spaceflight with EP devices was to great. Shortly thereafter Spitzer proved that Shepard and Clever's assumption for acceleration was too high. Recalculating it with a lower, more accurate acceleration value, Spitzer proved that EP was a viable option. Building off those who came before him, in 1954 Stuhlinger developed the standards for EP as a legitimate area of study [3].

EP devices encompass a wide variety of thrusters which can be broken up into three categories. The first, electrothermal devices, includes arcjet and resistojets, and they are any device where the propellant is electrically heated and expanded through a nozzle. Second is electrostatic propulsion where ions are accelerated by electric fields. The most common electrostatic devices are Hall thrusters and gridded ion engines. This category also includes field emission electric propulsion devices. The last category is electromagnetic thrusters. These devices use the Lorentz force to accelerate ions. Pulsed plasma thrusters and magentoplasmadynamic thrusters are placed in this category.

EP devices of particular interest in this research are the gridded ion engines and Hall thrusters, both of which utilize hollow cathodes as an electron source for ionizing the propellant and neutralizing the plume. Hollow cathode assemblies (HCA), shown in Figure 1, are devices consisting of a cathode tube, orifice plate, heater, keeper electrode, and insert material.

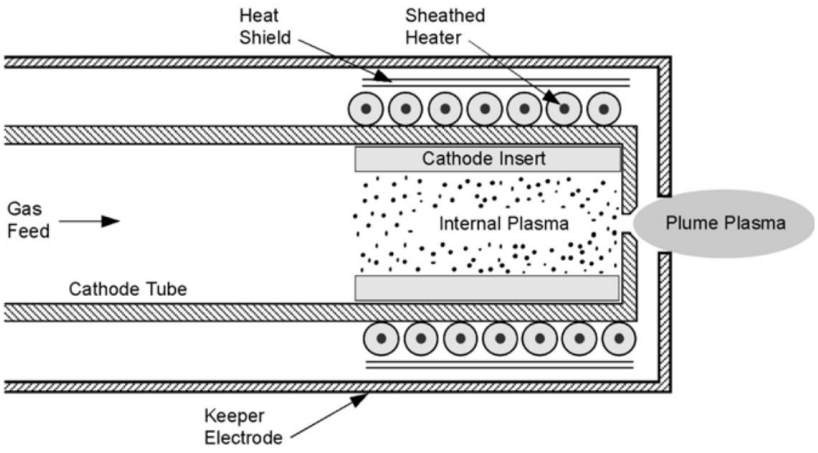

Figure 1 - Schematic of a hollow cathode assembly with labelled components [1].

The heater is used to raise the insert material to a specific temperature based on the type of insert used. When heated the HCA produces seed electrons that collide with neutral particles in the thruster, creating ions. Those ions are then accelerated by strong electric fields within Hall thrusters and gridded ion engines to create thrust [1]. By accelerating positive ions, a potential builds between the spacecraft and thruster plume, which can lead to arcing and damaging of the spacecraft [4]. To prevent this, HCAs are used to provide electrons to neutralize the plasma plume; HCA used in this capacity are referred to as neutralizing cathodes. Gridded ion engines have two cathodes. One cathode is for ionizing the propellant and the other cathode is for neutralizing the plume. In Hall thrusters, both processes are performed with a single HCA.

In general, there are two modes of hollow cathode operations that are governed by geometric relations between the orifice plate and the keeper electrode construction and placement. These modes are the spot (quiescent-mode) and plume (noisy-mode) [1]. The modes relate to the power required to sustain discharge and erosion rates that can limit HCA lifetime. The discharge current is the current that leaves the plasma and goes back through the anode. It comprises of electron and ion current and electron loss. Orifice geometry plays an important role

in determining plasma properties. Three orifice geometries are shown in Figure 2 [1]. Type A cathodes have an orifice with a large length-to-diameter ratio. This flow restriction causes ions and electrons to bombard the orifice walls, depositing their energy, and causing orifice heating. The small orifice diameter ultimately limits the discharge current. Type B cathodes have an orifice with a small length-to-diameter ratio and are heated by electron and ion bombardment of the insert. Lastly, type C cathodes have relatively no orifice and are heated by ion bombardment and usually supplemented with a heater during operation. Type C cathodes are used when high discharge current is required. Type A and B cathodes can be designed to self-heat. In other words, once the discharge in the HCA is sustained the heater can be turned off and the insert is heated by a combination of electron and ion bombardment and orifice heating.

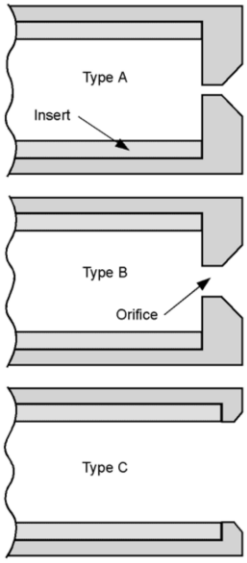

Figure 2 - Three orifice plate aspect ratio configurations [1]

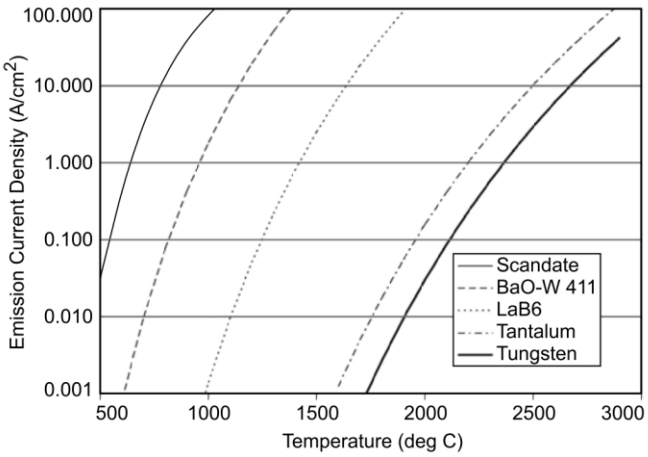

Figure 3 - Electron current density as a function of temperature for various insert materials [1].

Figure 3 shows emission current density as a function of temperature for several insert materials [1]. The work function is a temperature dependent material property. A low work function relates to the ease at which an insert will emit electrons. Barium Oxide (BaO) and Lanthanum Hexaboride (LaB_6) are the most common inserts materials used [5]. The low work function of BaO allows it to produce the same current density as LaB_6 with less energy input. BaO and LaB_6 insert materials have varying work functions that are related to manufacturing practices. Table 1 shows work functions of inserts that are discussed in this paper when available [1], [6], [7],[8].

Table 1 - Various work function for different materials.

BaO	2.06 eV
LaB_6	2.6 -2.9 eV
CeB_6	2.5 eV
Electride	0.6 eV

1.2 Research Motivation

Hollow cathodes continue to be the main source for providing seed electrons for gridded ion engines and Hall thrusters. A failure mode has been identified that is common in HCAs that

can limit mission lifetime. The cathode heater can fail as a result of excessive wearing of the keeper electrode during long-term operation, thus exposing the heater to high energy plasma. Or the heater can short due it excessive temperature cycles [9]–[12]. Another major concern is the improper handling of an emitter that can lead to emitter poisoning. Poisoning is a non-reversible process caused by the insert forming dipoles from the absorption of gases that react with the surface. This is typically more common in emitters that rely on chemical reactions to produce electrons, and it will drastically increase the work-function. BaO is at a high risk of becoming poisoned because it requires a barium dipole to react with the tungsten substrate to reduce the work function of the insert [13]. LaB_6 is considered at low-risk for becoming poisoned because it does not require chemical reactions to emit electrons. As a result, more care must be taken through the manufacturing process as well as during handling of experiments and travel when using BaO inserts [1].

Eliminating or minimizing failure-modes that are linked to excessive wear and improper handling can help increase hollow cathode lifetime for both deep space and orbital missions. Before time-consuming wear experiments are conducted on new insert materials a comparison of plasma properties between cathodes with different insert materials should be analyzed to determine whether further resources should be committed to studying a new insert material. This research presents comparisons of plasma properties experimentally measured with a Langmuir probe (LP) from cathodes operating with LaB_6, BaO, and a novel insert material called Cermet developed by Plasma Controls, LLC. The Cermet insert uses Paschen's law to initiate plasma breakdown without the need for a heater. It is also insensitive to poisoning, similar to LaB_6. Lastly, this thesis aims to increase the ability to perform plasma diagnostics in the Aerospace Laboratory for Plasma Experiments (ALPE) at Western Michigan University (WMU) by adding

a cathode internal probing (CIP) box. This resource will allow for a complete mapping of the cathode plasma structure using both insert and plume region data collected by a LP

1.3 Organization

This thesis is organized into several chapters to help guide the reader. Chapter 2 covers hollow cathode development as well as common (LaB_6 and BaO) and novel insert materials. Chapter 3 covers the methodology and experimental setup, including Langmuir probe theory. Chapter 4 presents experimental results, and Chapter 5 covers the conclusions and remarks about future work for the new Cermet insert material.

2 Background

2.1 Milestones in Cathode Development

Since cathodes are secondary components on EP devices they are traditionally developed to meet EP thruster requirements and in parallel with thruster development. Gridded ion engines, such as the Space Electric Thruster (SERT 1) and Program 661A, utilized hot tantalum filaments for both the main discharge and neutralization of the ion beam. The main discharge supplied sufficient seed electrons to ionize the plasma, but inconsistent neutralization of the plume was shown to be problematic; a spacecraft potential of -1000 V was reported for the Program 661A and test code B. Even though SERT 1 did report adequate neutralization of the ion beam using tantalum filaments, a more reliable source of seed electrons was required for repeatability of ion beam neutralization [4].

Discharge cathodes were extensively researched in 1967 by Reader and Pawlik [14]. The cathodes they tested are shown in Figure 4 and include brush-type, indirectly heated, and oxide-magazine cathodes. These cathodes were shown to operate with emission currents up to 10 A and for durations greater than >4000 hours. Unfortunately, each cathode showed an increase in power consumption up to 20 W/1000 hours over its life.

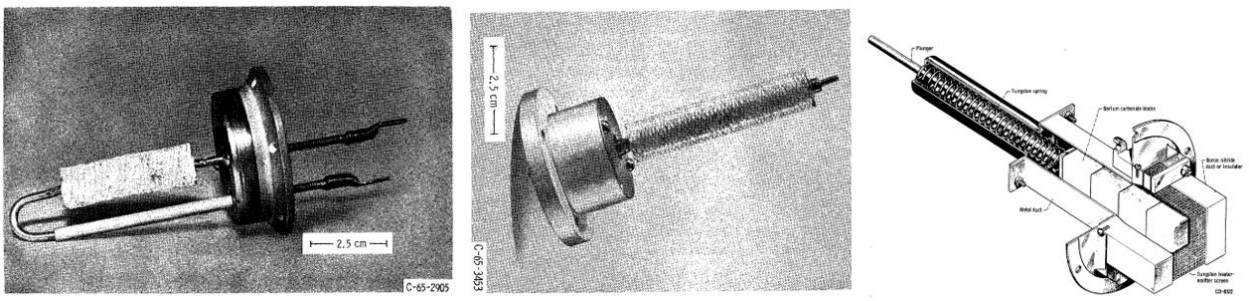

Figure 4 - Early construction of cathodes: Left) Brush type; Middle) Independent heated cathode; Right) Oxide-magazine cathode [14]

SERT 2 led the way for the development of a more reliable hollow cathode design and solved the neutralization problems that had been encountered up to this point. The same hollow cathode concept was used for both the main discharge and neutralization. This concept is schematically shown in Figure 5 and supplied up to a 2 A for the discharge and 0.25 A for plume neutralization. Both cathodes had been tested and were projected to last for over 10,000 hours of operation. This long life was achieved by having a low coupling voltage that reduced orifice and cathode tip sputtering, which can cause erosion [15].

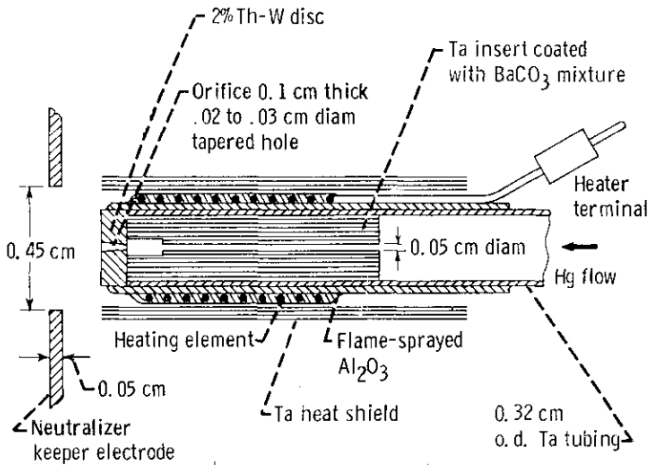

Figure 5 - Early constuction of hollow cathodes with labelled components [16].

In the mid-1980's the propellant for EP changed. Up to this point, mercury and cesium were the two main propellants, but due to environmental, safety, and spacecraft contamination concerns, a switch to inert gases was made [17],[18], [19]. Xenon, Krypton, and Argon were the leading propellants for investigation. The rest of the 80's and early 90's was used for life mission testing and component development.

Deep Space-1 was a technology demonstration mission that included gridded ion thrusters. The cathode extended life test proved that it could operate for over 30,000 hours with a

maximum flow rate of 3.7 sccm at low discharges (< 15 A) [1]. The satellite was launched in 1998 and was considered a success.

2.2 Insert Development

Early cathode inserts were composed of rolled tantalum foil to emit electrons and sustain discharge. These inserts proved to be unreliable for long duration on-off cycles that are often required for EP missions. Later, the rolled tantalum foil was coated with oxide. This provided a more reliable cathode with high on-off ignition cycles. Hudson and Weigand, investigated the reliability of impregnated tungsten inserts as a viable option for replacing the rolled-foil, oxide-coated inserts [20]. Their research concluded that the impregnated insert provided the same operational characteristics, but with improved on-off ignition cycles (> 900), machinability, uniformity, and evaporation rate control. The insert was composed of a 4:1:1 ratio of barium oxide, calcium oxide, and aluminum oxide. Today, this is a common molar ratio for BaO impregnated cathode inserts [1].

Boride material was studied by Lafferty in 1950 [21]. Lanthanum, cesium, and cerium were among the metals in which boride was mixed, forming XB_6 compounds. Lafferty determined that LaB_6 was far superior in both emission current and evaporation rates compared with other XB_6 insert materials. Gallagher found that LaB_6 poisoning was a function of pressure and temperature and has 2-3 orders of magnitude higher poisoning pressure than BaO [22]. Poisoning pressure refers to the pressure at which an insert begins to become poisoned. For LaB_6 at 1570 °C, the poisoning pressure is 10^{-3} torr. In comparison, BaO is reported to have a poisoning pressure of 10^{-5} and 10^{-3} torr at 1125 °C and 800 °C, respectively.

As EP technology rapidly develops, the need for high power cathodes becomes necessary. For discharges above 15 A, early BaO impregnated tungsten cathodes experienced a drastic reduction in lifetime because they rapidly depleted the barium at the higher temperatures required for greater discharge currents. This made them inadequate for high power applications that included both ion and Hall thrusters requiring discharges up to 100 A [23]. In the early 2000s, high power BaO cathodes were tested but were considered inadequate for long-life high power thruster missions [24]. In that study, the orifice plate of the cathode exceeded the maximum allowable temperature (1150 °C) when sustaining discharge currents greater than 25 A [25]. In 2012, three cathodes with varying component dimensions were tested with BaO inserts. It was determined that a larger orifice diameter and shorter insert helped to keep the orifice plate under the allowable maximum temperature that reduced the exhaustion of barium [26]. This cathode was able to produce a 100 A discharge while maintaining an orifice temperature below 1150 °C [6]. Around the same time that the high power BaO cathode was developed a high power long-life LaB_6 hollow cathode was presented by Chu and Goebel [27]. Although LaB_6 has a higher work function than BaO it remains an attractive insert material option because of its insensitivity to poisoning and low evaporation rates.

2.3 Alternative Insert Materials

In 1980 Geobel tested a Lanthanum Molybdenum (La-Mo) emitter, and telemetry data were collected for over a 50 hour testing period [28]. The La-Mo emitter was able to achieve high discharge currents but plateaued at 200 A after 80 V. Initial experimental testing determined that the emitter did not experience any rapid evaporation but needed to be disassemble and cleaned after 40 hours.

At the Colorado State University, Lauren et al. developed a one stop fabrication process to manufacturer calcium aluminate $12CaO\text{-}7Al_2O$ (C12A7) electride hollow cathode inserts [8]. C12A7 is capable of starting, almost instantly at room temperature without a heater. Theoretical values show a lower cathode operating temperature and work function. The emitter was successfully operated for 50 hours with Xenon and 20 hours with iodine, and it did not react or show signs of degradation with reported discharge currents up to 15 A.

Warner et al [7] performed a low flow rate comparison on LaB_6 and Cerium Hexaboride (CeB_6). They reported that the CeB_6 insert performed similar to LaB_6 by producing the same electron current density and similar plume and spot modes. Eventually the CeB_6 became poisoned, and LaB_6 outperformed it. They also showed that LaB_6 is a viable option for future low flow rate applications.

Cermet, the novel insert reported on in this thesis, was developed by Plasma Controls, LLC. Ignition testing was performed at Colorado State University prior to sending the H6 variant HCA with a Cermet insert to WMU. Figure 6 shows the cathode keeper voltage vs. flow rate curve from those initial experiments. Since the Cermet cathode does not use a heater it requires high initial pressure to cause plasma breakdown. The plasma breakdown is then sustained, heating the cathode insert material itself. Colorado State University reported nominal flow rates of 3 – 10 sccm for keeper currents of 200 – 1500 mA, respectively. The Cermet HCA uses a novel porous ingot insert that is comprised of tungsten powder and a mixture of barium, calcium, and aluminum ceramics. There are other minor additives to improve the insert structure and function. Similar to LaB_6, the Cermet insert does not require special handling procedures because it is insensitive to poisoning mechanisms.

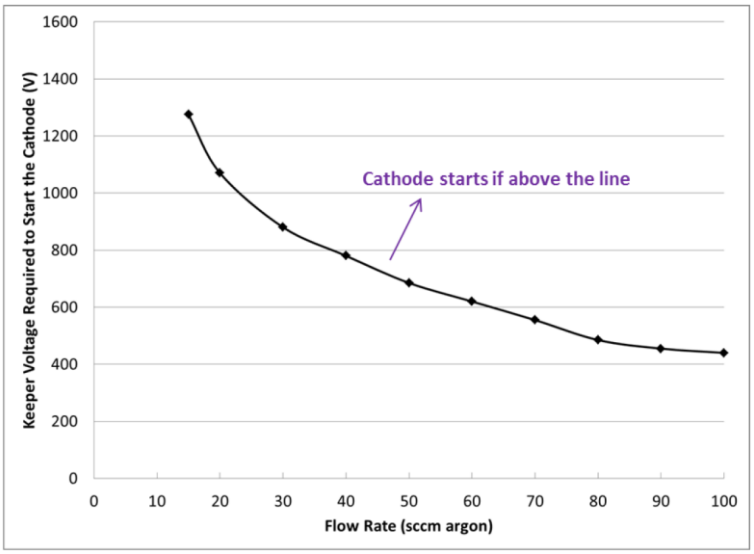

Figure 6 - Keeper voltage vs flow rate curve for starting the Cermet HCA.

3 Experimental Setup and Methodology

3.1 Langmuir Probe Theory

A single Langmuir Probe (LP) provides data that can be used to calculate ion number density, electron temperature, floating potential, plasma potential, and electron energy distribution function. The simple construction and well-studied analysis procedures make LPs an attractive option for plasma diagnostics. However, there are high levels of uncertainty in the final results. The uncertainty in electron temperature and plasma density can be up to 50% and 20%, respectively; however, these uncertainties drop significantly when comparing relative values using the same probing equipment [29]. These uncertainties are a combination of assumptions, probe construction, and alignment [30]. LP theory with a single cylindrical electrode is presented. For a more in depth understanding of probe geometry, best practices, and alternative LP diagnostics the reader is referred to ref [30].

LPs work by sweeping an applied voltage to the probe and measuring collected current. As the probe voltage, V_B, is biased with respect to the plasma potential, V_p, ions end electrons are collected to generate a probe current, I_p, thus producing an I-V curve shown in Figure 7.

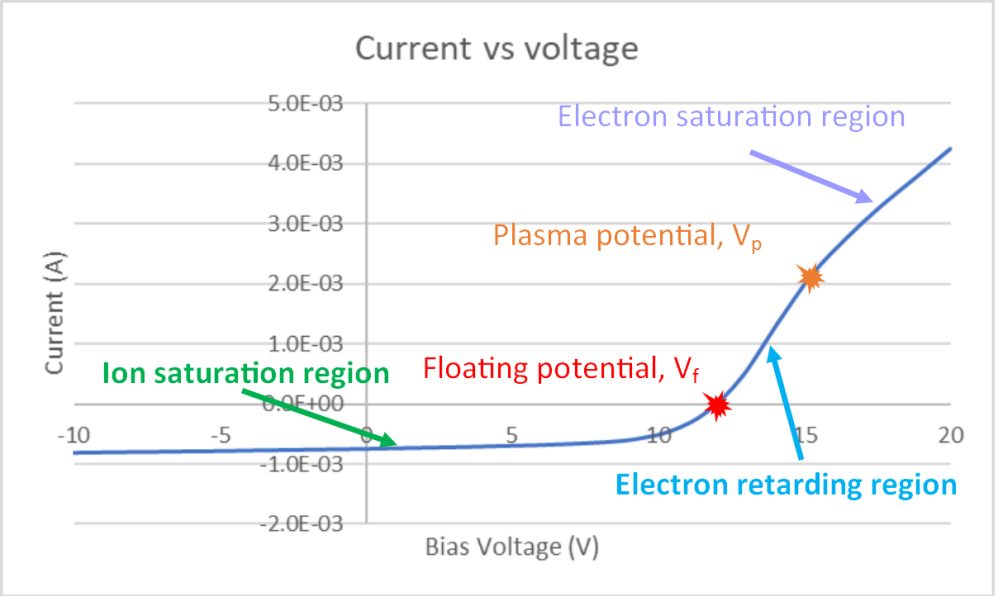

Figure 7 - I-V curve taken with a LP.

For $V_B < V_p$ ion current collection occurs. If the probe is biased sufficiently negative all electrons are repelled and ion saturation occurs. As the probe voltage is swept from negative to positive, the probe starts to shed ions and collect electron current. When the probe is collecting the same number of electrons as it does ions, the floating potential, V_f, is reached producing a net current of zero. If the probe voltage is sufficiently increased such that $V_B > V_p$, all of the ions are repelled and electron saturation is obtained. The area between the floating and plasma potential is referred to as the electron retarding region.

The electron current, I_e, is determined as a function of bias voltage,

$$I_e(V_B) = I_{e,sat}\exp\left(\frac{V_B - V_p}{T_e}\right) \qquad \text{Eq. 2}$$

where T_e is electron temperature.

Ion current collection is more complex then electron current collection and is dependent on sheath formation surrounding the electrode. The characteristic length of the sheath is called

the Debye length, λ_d. Once outside of the Debye length the plasma is unperturbed by the probe. The ratio of the probe radius-to-Debye length (r_p/λ_d) provides insight into how the ions interact with the sheath. The thin sheath criteria is met when this ratio is above 50 and thick sheath (or orbital motion limited, OML) criteria occurs when this ratio is below 3 [30]. The region between these two extremes is considered a transitional sheath. The following equations are used to calculate the ion saturation current, $I_{i,sat}$, based on the probe radius to Debye length ratio.

$$I_{i,sat} = -\exp\left(-\frac{1}{2}\right) e n_o A_p \left(\frac{eT_e}{m_i}\right)^{\frac{1}{2}}, \quad \frac{r_p}{\lambda_d} \geq 50 \qquad \text{Eq. 3}$$

$$I_{i,sat}(V_r) = \frac{eA_p n_0}{\pi}\left(\frac{2e(V_p - V_B)}{m_i}\right)^{\frac{1}{2}}, \quad \frac{r_p}{\lambda_d} \leq 3 \qquad \text{Eq. 4}$$

$$I_{i,sat} = eA_p n_o \left(\frac{eT_e}{2m_i\pi}\right)^{\frac{1}{2}} a \left(\frac{V_p - V_B}{T_e}\right)^{b}, \quad 50 \geq \frac{r_p}{\lambda_d} \geq 3 \qquad \text{Eq. 5}$$

$$a = 1.18 - 0.00080\left(\frac{r_p}{\lambda_d}\right)^{1.35} \quad b = 0.0684 + \left[0.722 + 0.928\left(\frac{r_p}{\lambda_d}\right)\right]^{-0.729}$$

where m_i is the mass of the ion.

The electron temperature is found by isolating the electron retarding region with the floating and plasma potential as its lower and upper bounds, respectively. The plasma potential is the voltage at which the "knee" occurs in Figure 7. Once the electron retarding region is bounded by the plasma and floating potential the electron temperature in electron volts is equal to the inverse slope of the natural log of the electron current vs. the probe voltage in that region.

3.2 Facilities

All testing was performed at WMU's ALPE. The vacuum chamber at ALPE measures 1.5-m long and 1-m diameter and uses a Brooks CTI-250 cryopump with a pumping speed of

1800 l/s Argon. The facility has the ability to attain high vacuum with a base pressure less than 10e-7 torr. High purity argon (99.999% pure) gas was used for all experiments, and flow was delivered by an Alicat scientific mass flow controller with a 0-100 sccm range. The vacuum chamber is outfitted with a residual gas analyzer, an RGA 100, from Stanford Research Systems to determine partial pressures of gas molecules at high vacuum. Two 600-5.5 and one 100-15 Lambda Genesys power supplies were used to power to the cathode keeper, discharge, and heater, respectively. The power supplies were controlled with a custom telemetry LabVIEW VI.

3.3 Hollow Cathodes Assemblies

The H6 HCA provided by JPL and the HCA provided by Plasma Controls, LLC, both shown in Figure 8, have similar, but not identical geometry. Table 2 compares common dimensions between the two cathodes. The H6 HCA was used with the LaB_6 insert and 4:1:1 molar ratio BaO insert. Both inserts were the same size with an inner diameter of 3.8 mm by 25.4 mm long. For comparison, a schematic of the Plasma Controls cathode is shown in Figure 9.

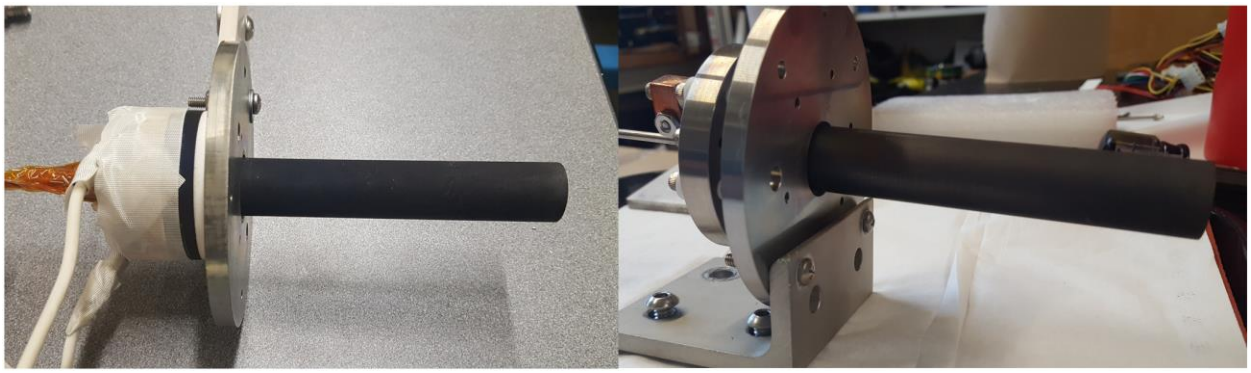

Figure 8 - HCAs used in the experiment. Left) Plasma Controls Right) JPL

Table 2 - Geometrical ratios of the HCA

HCA	Keeper diameter to orifice diameter ratio	Cathode tube diameter to orifice diameter ratio	Orifice plate to keeper gap distance ratio between HCA
JPL	2	2.34	7.0
PLC	2.29	4.53	

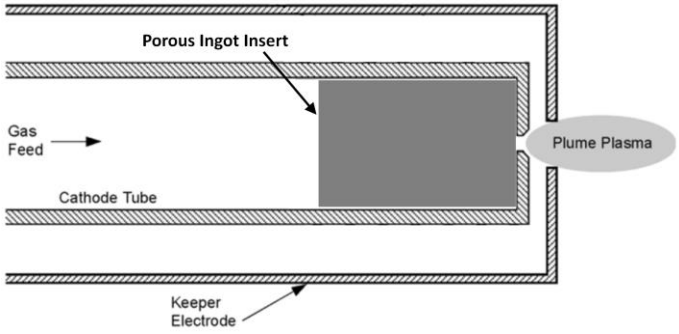

Figure 9 - Schematic of Plasma Controls H6-type HCA

3.4 Methodology

3.4.1 Overview

Part of this thesis work is to add the capability of making internal cathode or insert region measurements with an LP to ALPE. This thesis includes data from two experimental setups: one experimental setup was used to collect plasma properties and telemetry data for all three inserts using both HCA; the other experimental setup utilized the cathode internal probe (CIP) box to collect insert region plasma properties along with plume region plasma properties of the LaB_6 insert and HCA. Internal cathode data were collected at the same operating conditions as external LP data for the LaB_6 HCA only. This is because of the robustness of the LaB_6 insert material and cathode geometry.

3.4.2 Experimental Setup

Two computers running 4 different LabVIEW programs were used for the experiment. The first computer ran the telemetry VI. It provided the ability to automatically change the flow rate, discharge current, and keeper current, while recording the DC components of the voltage and current supplied to the keeper and anode as well as flow rate and pressure for post-processing. Data were collected at a rate of 10 kHz using a USB X-6356 NI DAQ. This VI ran the entire experiment, monitoring the device under test. Later these data were used to generate the keeper current-flow rate-discharge voltage (IVm) maps. The other computer ran the remaining three VIs, as required by the experiment. One was used to collect differential probe and Pearson coil data from the oscilloscope to measure the AC components of voltage and current supplied to the discharge and keeper. The other two VIs controlled the insert-region and plume-region motion tables and the source meter. A linear Velmex table with a total travel of 38 cm was used to move the plume region LP axially with respect to the cathode. A Thorlabs DDSM100 with a total travel of 10 cm was used to move the insert-region LP within the CIP box.

The CIP box was machined in-house at WMU from of a 30 cm by 10 cm by 15 cm aluminum cube, and it had a Plexiglas top. A gasket was made from Viton and used as a seal between the aluminum body of the CIP box and the top. It was electrically connected to the grounded cathode tube. The cathode heater was connected inside the CIP box while the keeper was electrically connected outside. Figure 10 shows photograph of the CIP box with label components.

Figure 10 -Internal probe box without the cathode, seal, and plexiglass top.

A Keithley 2400 was utilized as the source meter for biasing the LP and measuring collected current. A TDS 2014C Tektronix oscilloscope monitored cathode keeper and discharge current and voltage characteristics. Two Micsig DP10013 differential probes measured voltage and two Pearson coils measured current; the keeper used a 1 A/1 V Pearson coil and the discharge used a 10 A/1 V Pearson coil. Figure 11 shows the electrical schematic of the experimental setup, including the differential probes and Pearson coils. As the Cermet cathode does not require a heater, this power supply and vacuum feedthrough were not used during Cermet testing. During operation of the BaO and Cermet HCAs, the circuit protection shown in Figure 11 that included diodes and a current limiting resistor was utilized. The circuit protection suppressed arcing and protected the power supplies during operation. The LaB_6 insert did not require this protection, as it had previously been studied in ALPE.

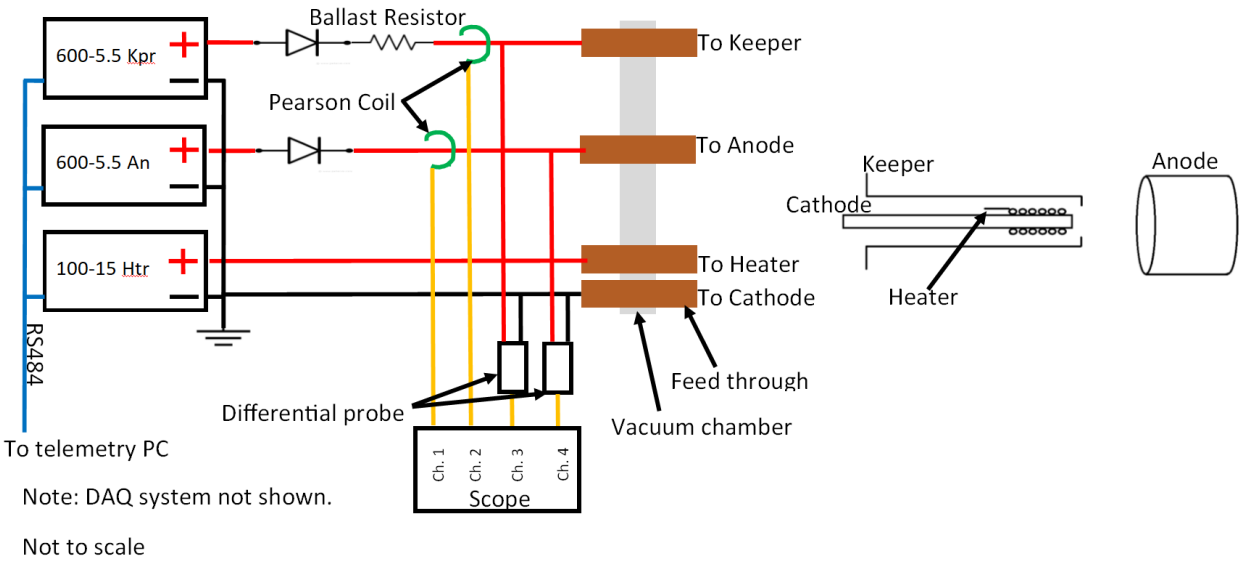

Figure 11 - Electrical configuration of HCA setup.

The physical experimental layout inside the vacuum chamber is shown in Figure 12. Table 3 provides the location of each cathode with (when available) and without the CIP box. A 10.1-cm-diameter by 25.4-cm-long stainless steel anode was placed such that the edge of the anode and the face of the keeper were in the same plane and the anode was concentric with the keeper tube for all HCA experiments. When the LP is not used it remains at 38 cm from the cathode orifice plate. This is the total travel distance of the Velmex table.

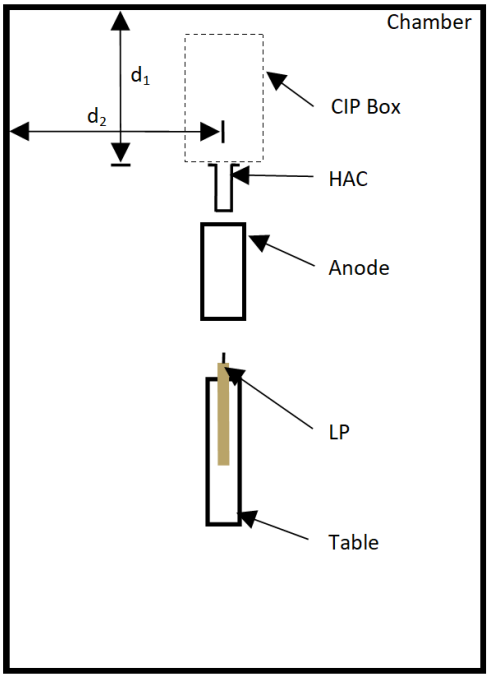

Figure 12 – Experimental layout inside vacuum chamber.

Table 3 - Cathode placement inside vacuum chamber.

Insert	With CIP box		Without box	
	d_1 (cm)	**d_2 (cm)**	**d_1 (cm)**	**d_2 (cm)**
BaO	--	--	20	51
LaB_6	41	51	20	43
Cermet	--	--	20	58

3.4.3 Telemetry Data

.To ensure consistency in collected telemetry data, the telemetry VI is capable of autonomously running through the combination of flow rates, discharge currents, and keeper currents in Table 4The VI also has the ability to restart the cathodes at predetermined conditions. If cathode discharge was not sustained after three attempts the next operating point was tested. When switching operating points two or five minutes were allowed to lapse for a current or pressure change, respectively, before the telemetry VI recorded any data. If the operating point was stable with a sustained discharge, the telemetry VI averaged ten measurements of flow rate,

pressure, keeper voltage, keeper current, discharge voltage, and discharge current. Single measurements of peak-to-peak keeper voltage and current and discharge voltage and current were recorded after the time lapse as well.

Table 4 - Operating points tested for each HCA.

Operating point	Flow rate (sccm)	Keeper current (A)	Discharge current (A)
1	6	1.5	4
2	6	1.0	4
3	6	0.5	4
4	6	1.5	3
5	6	1.0	3
6	6	0.5	3
7	6	1.5	2
8	6	1.0	2
9	6	0.5	2
10	6	1.5	1
11	6	1.0	1
12	6	0.5	1
13	6	1.5	0
14	6	1.0	0
15	6	0.5	0
16	4	1.5	4
17	4	1.0	4
18	4	0.5	4
19	4	1.5	3
20	4	1.0	3
21	4	0.5	3
23	4	1.0	2

Operating point	Flow rate (sccm)	Keeper current (A)	Discharge current (A)
24	4	0.5	2
25	4	1.5	1
26	4	1.0	1
27	4	0.5	1
28	4	1.5	0
29	4	1.0	0
30	4	0.5	0
31	2	1.5	4
32	2	1.0	4
33	2	0.5	4
34	2	1.5	3
35	2	1.0	3
36	2	0.5	3
37	2	1.5	2
38	2	1.0	2
39	2	0.5	2
40	2	1.5	1
41	2	1.0	1
42	2	0.5	1
43	2	1.5	0
44	2	1.0	0
45	2	0.5	0

3.4.4 Langmuir Probe Data

Common operating conditions were selected at which LP data would be collected for the insert and plume region for stable operating points. Internal and external LP data were measured at 2-mm axial intervals beginning 40 mm from the orifice plate and ending exit plane of the orifice plate. Both the internal and external LP were constructed using a 250 μm diameter tungsten wire that was 6.35 mm and 2.07 mm long for the external and internal probe, respectively. The speed of each IV curves were determined by the number of lines per cycle (NPLC). The NPLC was set to 0.1 and 1 for the internal and external regions, respectively, at 60

Hz. Common LP theory previously discussed was used to process the insert and plume-region data [30].

4 Results and Discussion

4.1 Ignition

Each insert has its own startup procedure to initiate plasma breakdown. The LaB_6 and BaO use a heater to bring the insert up to the required temperature, but the BaO has a lengthy conditioning and activation process. The Cermet inserts does not require a heater and utilizes Paschen's law to initiate breakdown; by increasing the cathode's internal pressure, an arcing event occurs between the keeper and cathode which causes breakdown to occur.

4.1.1 LaB_6

Starting the LaB_6 HCA is a very straight forward process. Once the chamber reached a total pressure of below 1e-5 torr, the keeper current and discharge current were set to 1.5A and 4 A, respectively. The LaB_6 cathode was heated to 198 W before the nominal gas flow was set to 6 sccm. Shortly after gas flow was initiated, plasma breakdown occurred and discharge was sustained.

4.1.2 BaO

BaO cathodes require a lengthy conditioning and activation process before starting the cathode. The conditioning process is to help prevent poisoning of the dispenser insert. Once the chamber pressure reaches 10e-7 torr the conditioning of the insert can begin. The heater was stepped up from 0 A to 7 A in 1 A incremental steps. The heater current was held constant for 1 hour at both 4 A and 7 A while outgassing was observed. During this process the residual gas analyzer was used to monitor oxygen, water, and carbon monoxide at atomic mass numbers of 18, 44, and 16, respectively. Figure 13 shows the outgassing of these monitored molecules during the conditioning process. If an increase in these elements was observed, heater power was

held constant until the partial pressure dropped back down to the partial pressure that was observed before the spike. At any time during cathode conditioning, if a total pressure of 1e-6 torr was reached in the vacuum chamber the heater was turned off until a pressure of 6e-7 torr was reached before continuing the conditioning process.

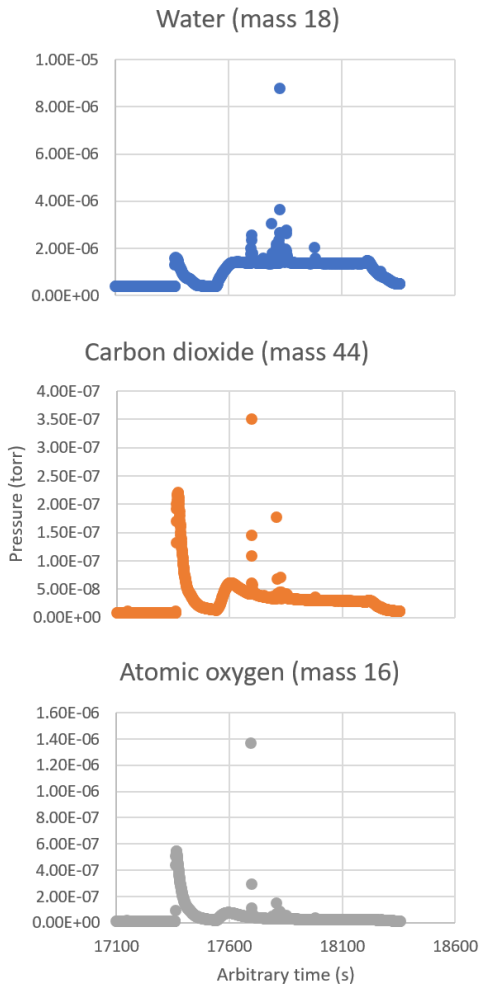

Figure 13 - RGA100 monitoring results during conditioning process of the BaO insert within the HCA .

After the conditioning process was complete, the heater was turned off, and the insert was allowed to cool for 30 minutes. Then, the heater was turned back on at 7 A and the emission current was recorded as the insert was heated. The emission current as a function of time is shown in Figure 14. The Keithley 2400 sourcemeter was connected to the anode and set to 100 V

while measuring the current. The final emission current values were lower than expected when comparing them to similar experiments in literature; however, this did not affect cathode ignition [31]. After conditioning, the cathode was started by setting the keeper current, discharge current, and flow rate 1.5 A, 4 A, and 6 sccm, respectively.

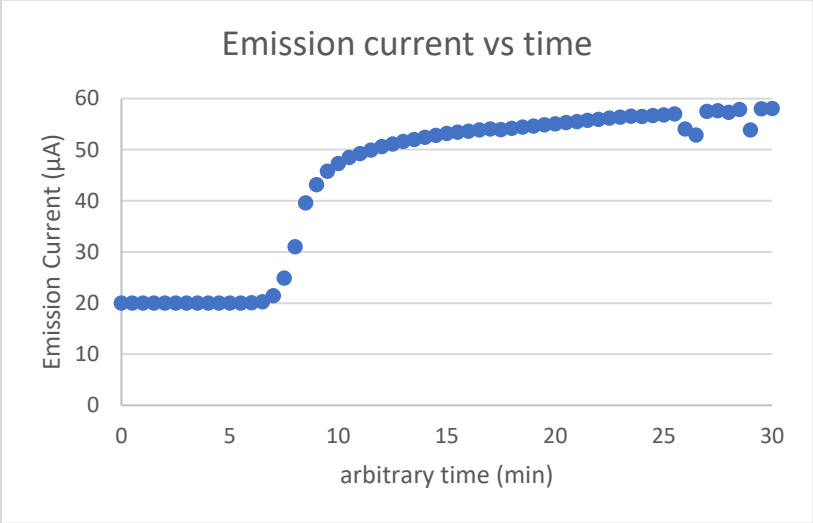

Figure 14 - Emission current of the BaO cathode recorded while heating the insert after conditioning.

4.1.3 Cermet

Starting the Cermet cathode does not require a heating process. Once the vacuum chamber pressure was below 10e-5 torr the ignition process began. The Cermet cathode uses the principles of Paschen's law, igniting an electrical breakdown inside the cathode tube through a combination of pressure and a strong electric field. To increase the internal pressure of the cathode to initiate gas breakdown, the flow rate of argon to the cathode was increased. The startup process is as follows: (1) set the cathode keeper and discharge power supplies to 600 V at 1.5 A and 90 V at 4 A, respectively; (2) set the argon flow rate to 100 sccm and hold for 3-5 seconds; (3) reduce the flow rate to an operating flow rate of 6 sccm. If the cathode shut off for any reason it could take up to 3 hours before it would start again. However, since this anomaly

with starting the cathode was not reported with the initial testing done by Colorado State University, it is thought to be caused by thermal issues with diodes in the protection circuit.

4.2 External Probing Results

Processed telemetry and LP are presented for each insert material. Table 5 shows the stable operating points that were identified for each insert. The shaded boxes are where LP IV curves were measured. LP data were only collected for discharge currents of 4 A and 2 A at the following keeper current/flow rate combinations: 1.5 A/6 sccm, 1.0 A/6 sccm, 1 A/4 sccm, and 1.5 A/2 sccm. LP data were not collected for all insert materials at all of the combinations listed above. For instance, the LaB_6 HCA was made unstable by the presence of the LP at the 2 A/6 sccm operating condition. As a result, these points could not be analyzed.

Table 5 - Stable operating points marked with "X." Shaded box is where LP data were collected.

Current (A)	Keeper	1.5			1.0			0.5		
Anode	flowrate (sccm)	LaB_6	BaO	Cerm	LaB_6	BaO	Cerm	LaB_6	BaO	Cerm
4	6	X	X	X	X	X	X	X	X	X
	4	X	X	X	X	X	X	X		
	2	X								
3	6	X	X	X	X	X	X	X	X	X
	4	X	X	X	X	X	X	X		
	2	X								
2	6	X	X	X	X	X	X	X	X	X
	4	X	X	X	X	X	X	X	X	
	2	X	X			X				
1	6	X	X	X	X	X	X	X	X	X
	4	X	X	X	X	X	X	X		
	2	X	X			X			X	
0	6	X	X	X	X	X	X	X	X	X
	4	X	X	X	X	X				
	2		X			X				

4.2.1 Telemetry

The telemetry data are presented in Appendix A. From these data current-voltage-mass flow rate (IVm) maps for each cathode insert were created. The IVm maps for each insert are shown in Figure 15 - 16 for a discharge current of 4 A. The red dots show were telemetry data were recorded. Interpolation was used between the operating points to generate the surface. The x-axis is keeper current, the y-axis is mass flow rate, the z-axis is discharge voltage, and the discharge peak-to-peak voltage makes up the color mapping. These maps can be used to determine a best-fit cathode for a thruster. For instance, the LaB_6 HCA provides a better overall range for operation, but if operated with a discharge current of 4 A, keeper current of 0.5 A, and a flow rate of 4 sccm the cathode to discharge coupling could lead to high peak-to-peak voltages. This could strain the power supply and produce high energy ions that could accelerate erosion [1]. IVm maps for the remaining anode current conditions are located in Appendix A.

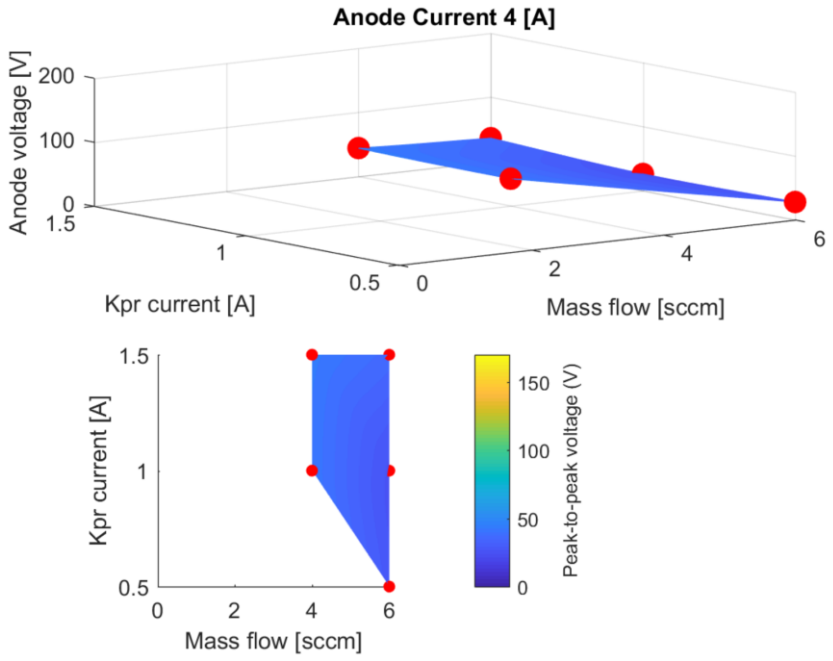

Figure 15 - BaO IVm map at an discharge current of 4 A. Red dots depict where telemetry was taken.

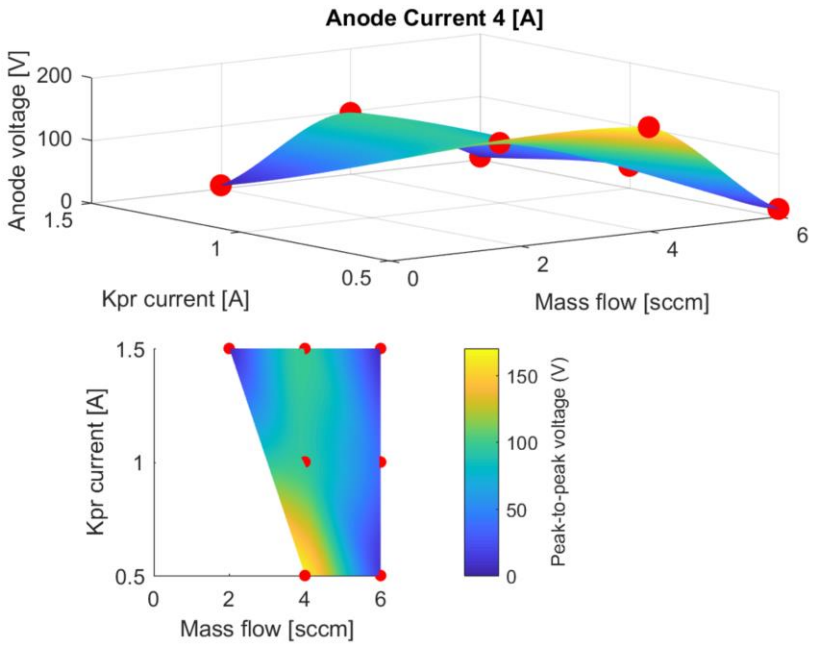

Figure 16 - LaB_6 IVm map at an discharge current of 4 A. Red dots depict where telemetry was taken.

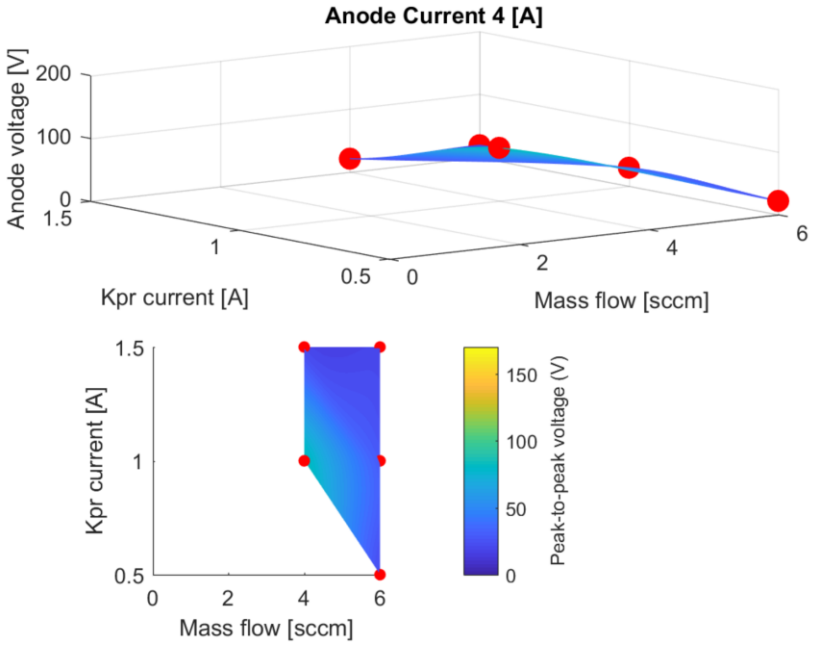

Figure 17 - Cermet IVm map at an discharge current of 4 A. Red dots depict where telemetry was taken.

Figure 18 – 20 represent the total power required to run each cathode at each operating point. For these figures, if a total current has two power levels for a single flow rate, the square data points represent where 1.5 A was supplied to the keeper and the circle data points represent

where 0.5 A was supplied to the keeper. For the telemetry data gathered the LaB_6 and Cermet power levels are not relatively affected by flow rate until a total current level of 4.5 A is required to sustain discharge. The BaO power levels are influenced by the current supplied to the keeper for the same total current used to sustain discharge. For instance, at 6 sccm and with a total current of 1.5 A supplied to the cathode, the power required to sustain discharge is not constant. When 1.5 A is supplied to the keeper and 0 A is supplied to the anode, the total power supplied to the cathode is 228 W. Whereas when 0.5 A is supplied to the keeper and 1 A is supplied to the cathode the total power is reduced to 88 W.

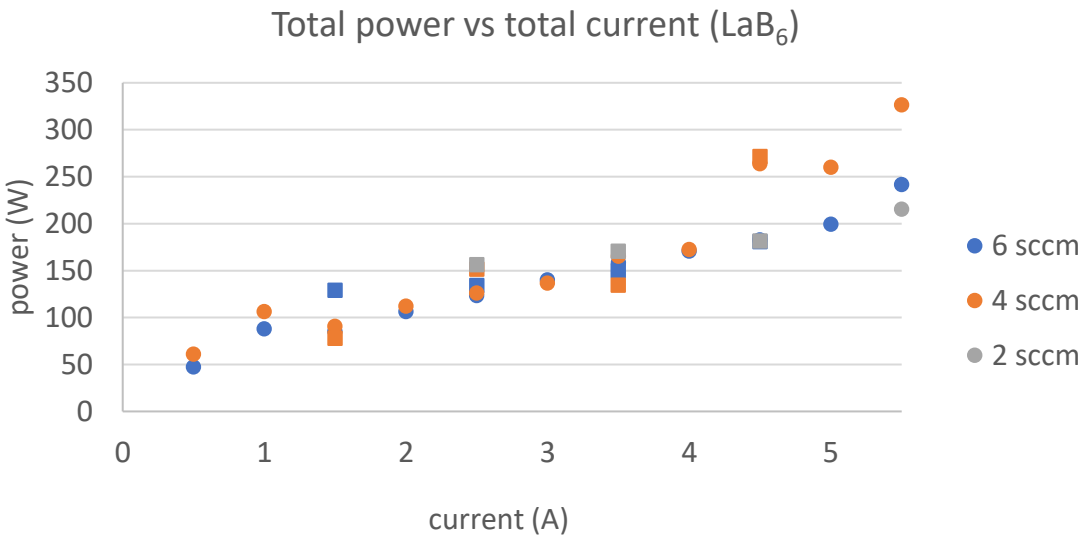

Figure 18 - Total power vs total current for the LaB_6 insert. Single data points that had multiple total currents and used 1.5 A for the keeper is represented by a square data point.

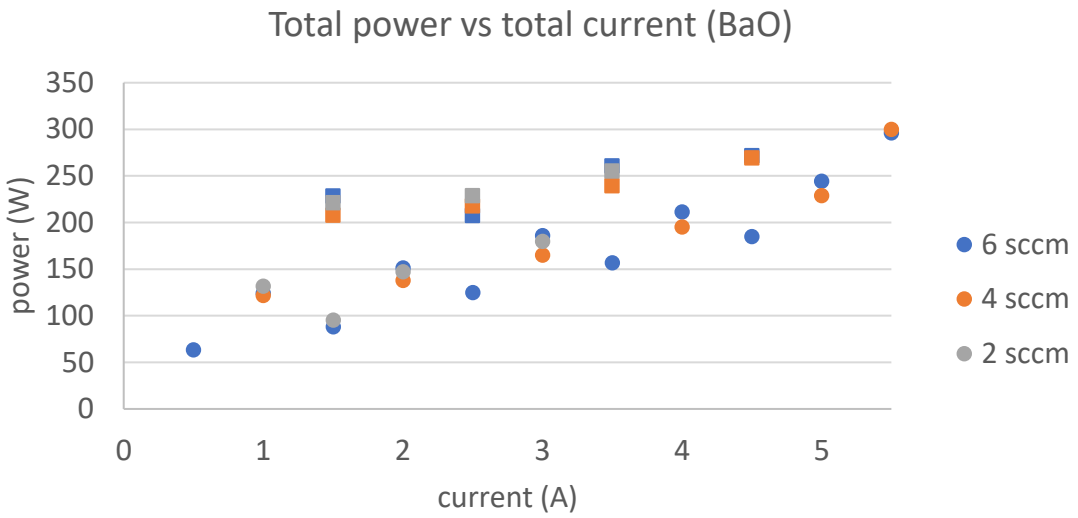

Figure 19 - Total power vs total current for the BaO insert. Single data points that had multiple total currents and used 1.5 A for the keeper is represented by a square data point.

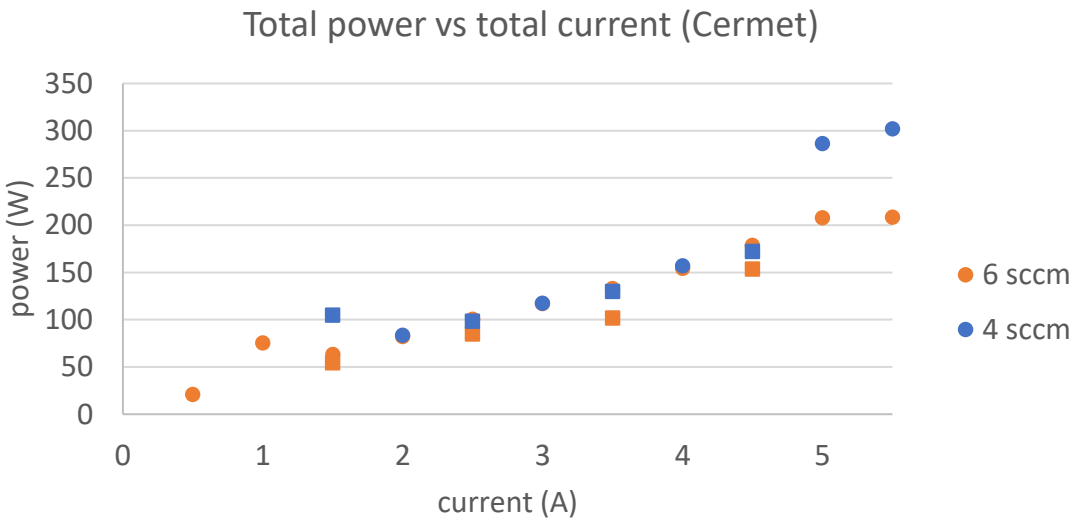

Figure 20 - Total power vs total current for the Cermet insert. Single data points that had multiple total currents and used 1.5 A for the keeper is represented by a square data point.

4.2.2 Plasma Properties

The probe radius-to-Debye length ratio never exceeded one; therefore, OML theory was used during all post-processing of LP data. Only the LP IV of stable operation was analyzed. If

an arcing event occurred or if the cathode shut off during LP operation those data points were discarded. The plasma property graphs were generated from the tables from Appendix B.

For the LaB_6 insert, plasma potential and ion number density are presented in Figure 17 as a function of downstream position at two operating points: 6 sccm flow rate, 1.5 A keeper current, 4 A discharge current and 6 sccm, flow rate, 1 A keeper current– 1 A, 4 A discharge current. The electron temperature ranged from 1.9 - 5 eV. For each respective flow rate, the electron temperature remained relatively constant. Holding the discharge current and flow rate constant produced an ion number density that was an order of magnitude lower for a keeper current of 1 A when compared to a keeper current of 1.5 A.

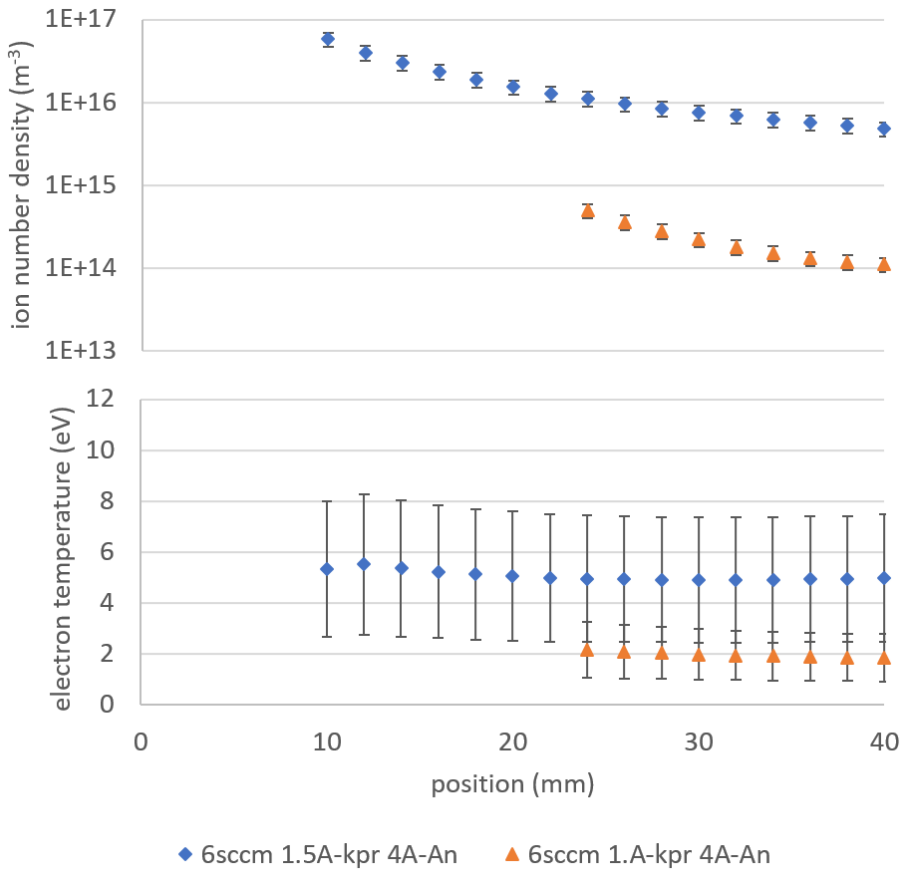

Figure 21 - LaB_6 plasma properties for different flow rates, keeper, and discharge levels. kpr = keeper; An = anode

For the BaO insert, plasma potential, ion number density, and electron temperature as a function of downstream location are shown in Figure 22 at the conditions given in Table 5. The plasma potential ranged from 12 to 37 V, and the electron temperature ranged from 3 to 5 eV. Unique trends to the plasma potential and electron temperature can be observed. By holding the discharge current constant at 2 A and the keeper current constant at 1.5 A, the electron temperature ranges from 5 eV near the orifice plate and decreases to 3 eV for 2 sccm; however, at 6 sccm the electron temperature ranges from 4 eV at the orifice plate and increases past 5 eV downstream. For the 2 sccm flow rate the plasma potential remains constant in the region probed, whereas in the 6 sccm condition the plasma potential follows the same trend as the electron temperature increasing from 31 V near the orifice plate to 38 V downstream.

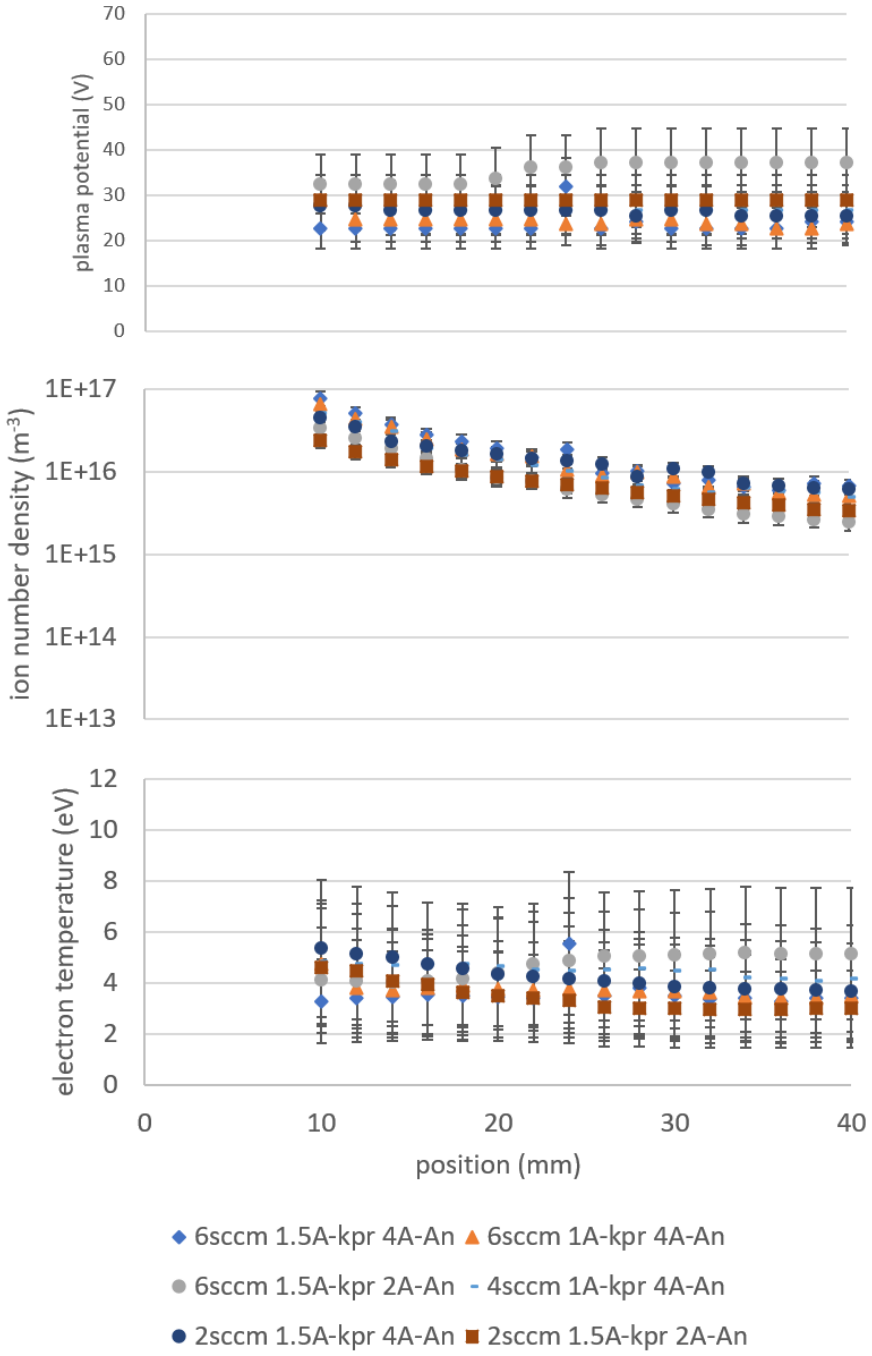

Figure 22 - BaO plasma properties for different flow rates, keeper, and discharge levels. kpr = keeper; An = anode

For the Cermet insert, plasma potential, ion number density, and electron temperature as a function of downstream location are shown in Figure 23. The plasma potential ranged from 25 V to 62 V, and the electron temperature ranged from 3 eV to 11 eV downstream. The plasma

potential and electron temperature vary widely over some operating conditions. This could be evidence of plume mode and plume to spot mode transition [26]. Several unique trends can be determined from the plasma property data. First, cathode keeper current has the least effect on cathode operation. This is observed when the mass flow rate and discharge current are held constant. It is also evident that higher flow rates combined with lower discharge currents produce constant plasma properties. Furthermore, there is a maximum electron temperature reached at approximately 15 mm downstream of the orifice plate for almost all operating conditions.

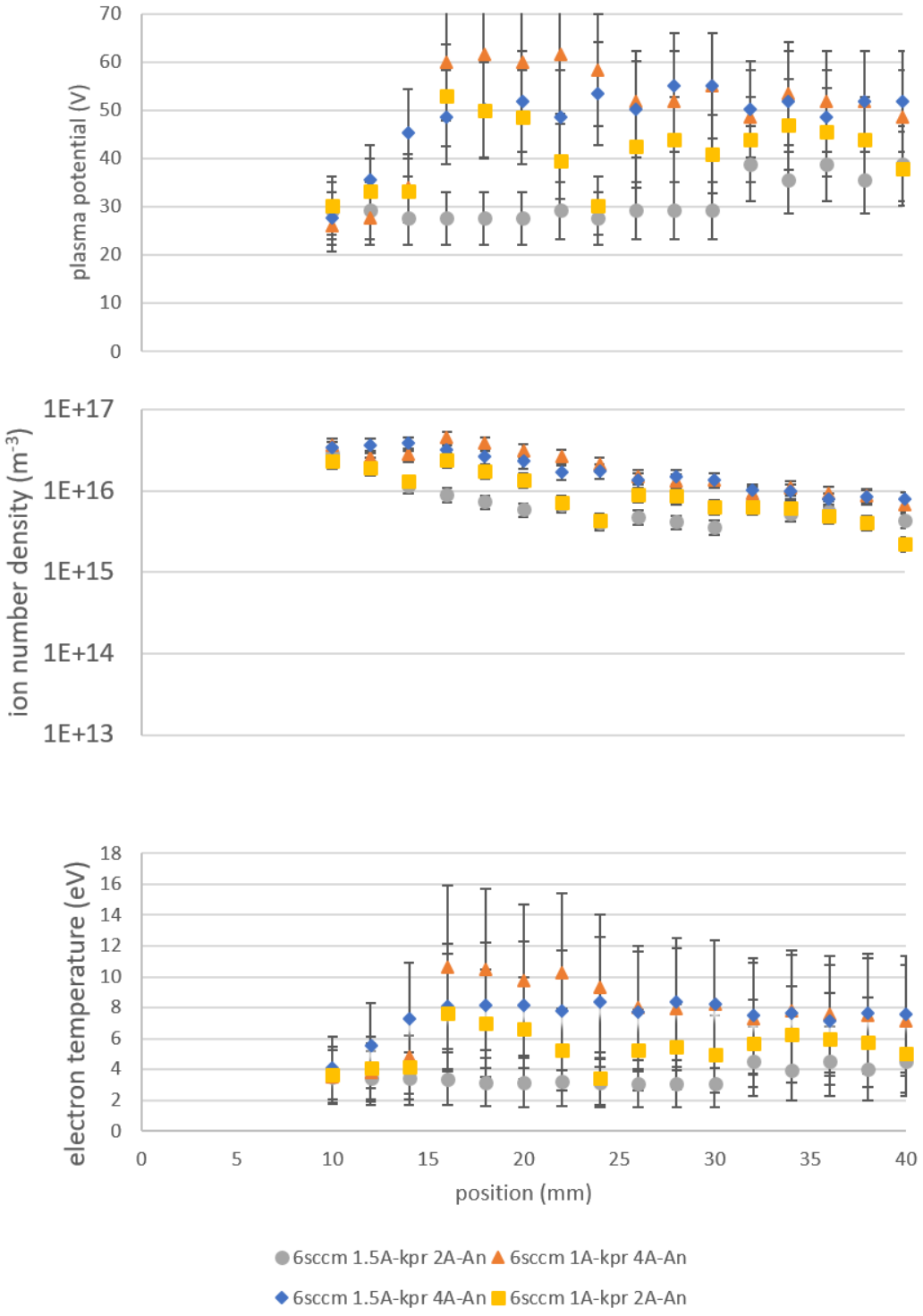

Figure 23 - Cermet plasma properties for different flow rates, keeper, and discharge levels. kpr = keeper; An = anode

For a better comparison of the ion number density between different insert materials, the densities from the LaB_6 (Figure 24) and BaO (Figure 25) cathodes are normalized with respect to the Cermet ion number density for similar operating points. The Cermet produces a higher ion number density than the LaB_6 insert for the data gathered. Referring back to the power graphs in the telemetry section, the reduction in the ion number density by the LaB_6 is a result of the reduced power drawn by the cathode. The Cermet power draw remains constant for both operating conditions. The BaO insert produces a higher ion number density than the Cermet between 10 to 25 mm downstream the orifice plate, but after 25 mm the Cermet ion number densities are comparable to the BaO. The Cermet cathode required less power to generate the ion density numbers shown in Figure 25 except, at the 4 sccm condition with 1 A and 4 A supplied to the keeper and anode, respectively.

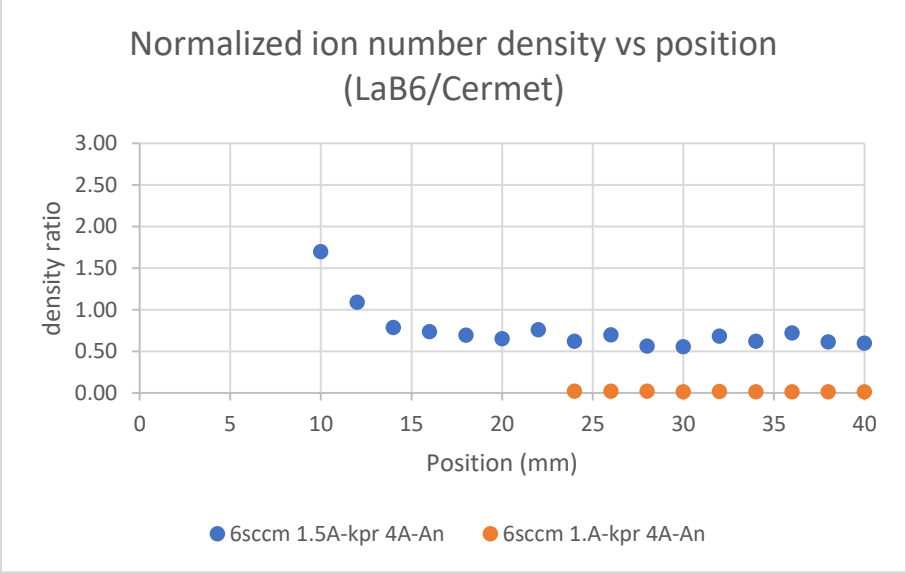

Figure 24 – Normalized ion number density of (LaB_6/Cermet) vs downstream position for various flow rates. kpr = keeper; An = anode

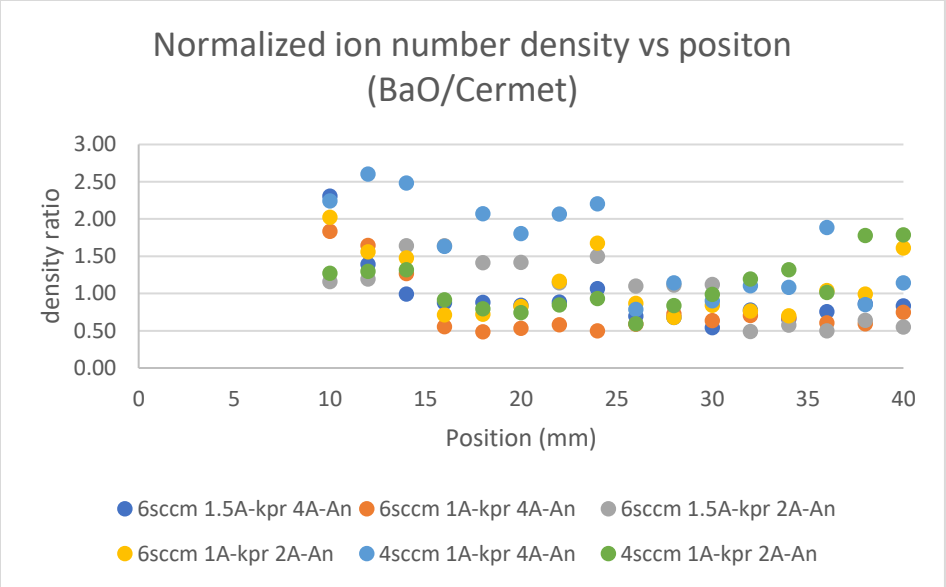

Figure 25 - Normalized electron number density of (BaO/Cermet) vs downstream position for various flow rates. kpr = keeper; An = anode

4.3 Internal Probing Results

All CIP box probe data were taken with a different LaB_6 insert provided by JPL because the original insert broke while removing it. Internal probing and external probing of the insert region of the LaB_6 HCA were attempted at similar operating conditions as those where data were collected externally without the CIP box. Only one stable operating point was found that coincided with both the external and internal probing: 6 sccm flow rate, 1.5 A keeper current, 4 A anode current. Figure 26 - 24 show the plasma properties for both the internal and external regions of the LaB_6 cathode operating at this condition. The electron temperature ranged internally from 1 eV - 5 eV and then increased to 6.5 eV outside the cathode before reducing to 4 eV further downstream. The plasma potential followed the same trend as the electron temperature. Internal to the cathode the plasma potential ranged from 5 V – 17 V and then decreased from 40 V to 30 V going away from the orifice plate. The electron density is higher in near the orifice plate for both the internal and external regions, demonstrating agreement with

previous experiments [1]. When comparing the electron temperature in the external plume region of the LaB_6 cathode with and without the CIP, it is possible that the CIP box may have influence on the plasma.

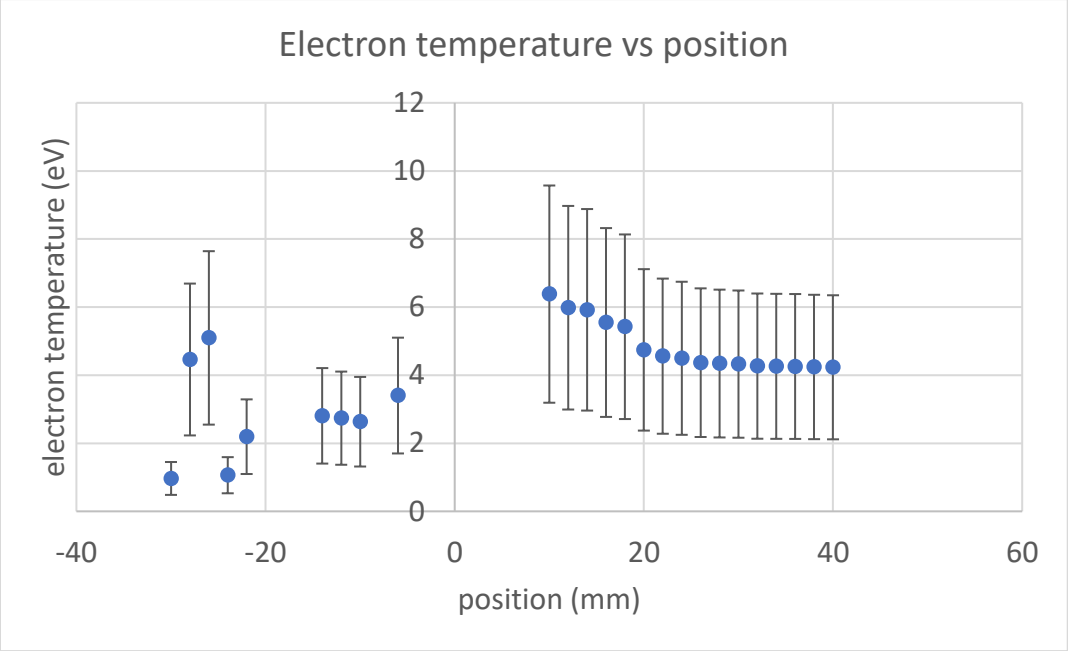

Figure 26 - Electron temperature as a function of position inside/outside the LaB_6 HCA.

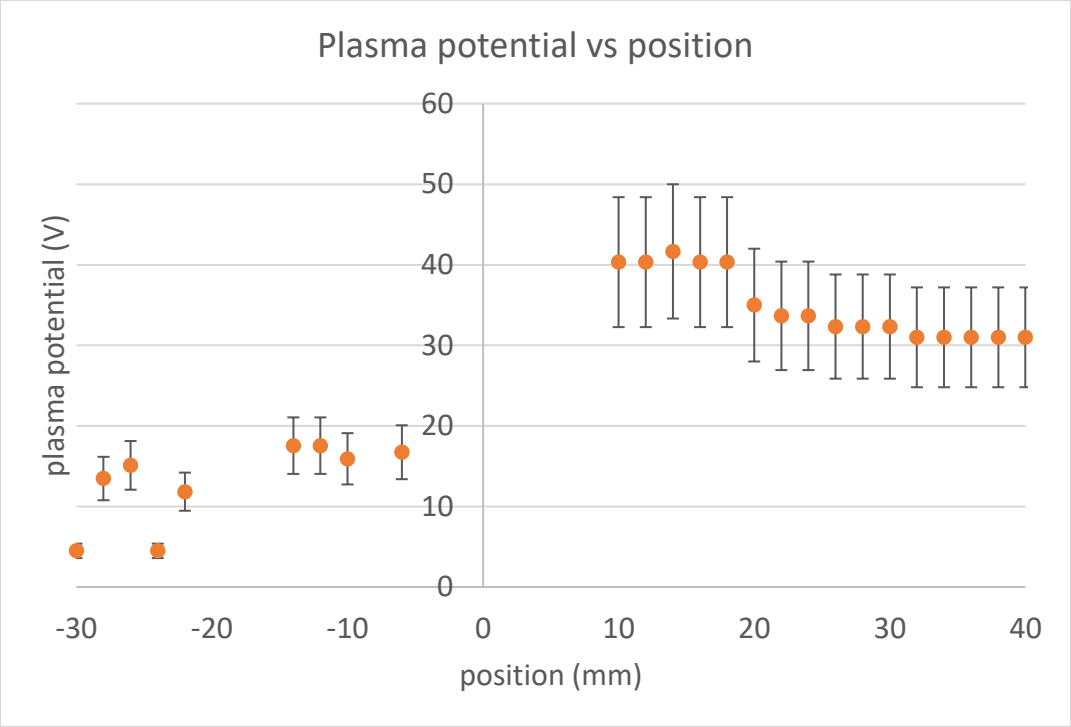

Figure 27 - Plasma potential as a funcition of poition inside/outside the LaB_6 HCA.

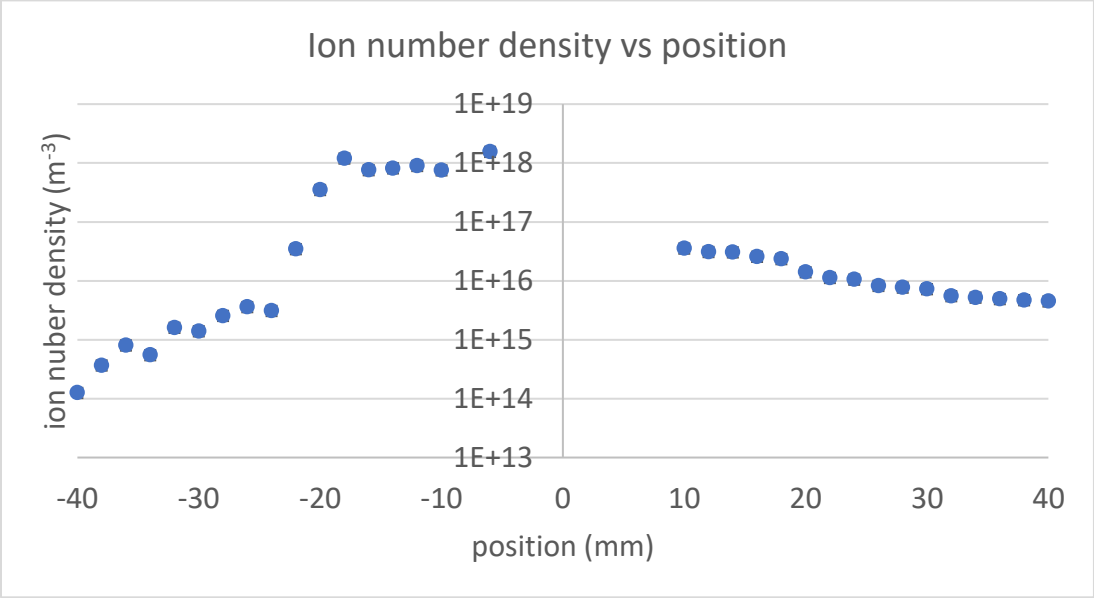

Figure 28 - Combined internal and external ion current density as a function of position inside/outside the LaB_6 HCA.

5 Conclusions and Remarks

Three inserts were observed in two different H6-type HCA configurations, BaO, LaB_6, and a novel insert material, Cermet. Two single LPs were used to determine electron temperature, ion number density, and plasma potential as a function of axial position, 10 mm – 40 mm downstream of the orifice plate in the plume-region for each insert. Telemetry data were gathered at varying flow rates, cathode keeper currents, and discharge currents. These are displayed in IVm surfaces that can help determine coupling operation with a thruster. An internal cathode probing box was built and tested on the LaB_6 insert. A single LP was used to determine electron temperature, ion number density, and plasma potential as a function of axial position upstream of the orifice plate for a single operating condition from 40 mm to 6 mm upstream of the orifice plate, and from 10 mm to 40 mm downstream of the orifice plate, in the plume-region.

Several conclusions can be drawn from the presented research. The HCA with the LaB_6 insert has the widest operating range over the combination of flow rates and currents that were tested. However, it also generated the largest peak-to-peak discharge voltage, which may lead to increased erosion of the cathode keeper surface. The HCA with the LaB_6 insert was also most influenced by the presence of the LP. This was evident by unstable operation or cathode shut down at certain operating points while measuring LP data.

The ion number densities for the BaO and Cermet inserts were not influence by the operating conditions. By normalizing the ion number density of the LaB_6 insert with the Cermet insert, it showed that the Cermet produced a higher ion number density than the LaB_6 insert. At a lower keeper current the cathode used less power causing the ion number density to reduce an order of magnitude. When normalizing the BaO insert with the Cermet insert, it was determined

that the BaO insert produced a higher ion number density than the Cermet from 10 mm to 25 mm downstream of the orifice plate; from 25 mm to 40 mm the Cermet is very comparable to the BaO insert. When comparing the ion number densities of the Cermet to the BaO insert the Cermet required less power for most of the operating conditions.

The LaB_6 cathode produced the lowest electron temperatures which were shown to be influenced by keeper current. The Cermet cathode showed an increase in electron temperature as a function of position. This temperature increase at certain operating conditions could be indicative of either spot mode or a transition from spot mode to plume mode. A maximum electron temperature for the HCA with the Cermet insert was observed approximately 15 mm downstream of the orifice plate for most of the cathode operating conditions. This could be a result of the increased distance between the orifice plate and keeper plate of the Cermet HCA and when compared to that of LaB_6/BaO HCA.

Successful internal probing of the LaB_6 HCA was completed with corresponding external plume data using the CIP box. The ion density trends shows good agreement with literature [1].

5.1 Future Work

This initial research of the Cermet insert inside an H6-type HCA shows that it can produce ion density comparable to that of H6 cathode with LaB_6 and BaO inserts. Thus, the Cermet cathode could be an attractive option for further investigation to determine if its viable for future use in EP devices. Future experiments should test the cathode at higher discharge currents where the results can be compared to the JPL H6 cathode, which was designed for high power operation. To extract information a single Langmuir probe on an x-y cartesian setup should be used to map the plasma properties around the cathode axially and radially. Laser

Induced Fluorescence can be used to determine if any high energy ions are present. Internal probing, once an open cylinder insert is available, will provide the plasma properties inside the cathode. Reducing the size of the ceramic used for the internal LP could lead to the cathode having more stable operating points, while internally probing the insert region. Placing the CIP in such a way to increase the line of sight, can provide visual confirmation that the motion table is behaving properly. Ignition studies and long term operational testing should be completed. Although not explored further in this experiment, repeatability of starting of the cathode should be further investigated. Lastly, determining how the geometry of the HCA affects operation and startup should be performed. This experiment will vary cathode orifice diameter and length, keeper orifice diameter, keeper to orifice plate gap distance, and cathode tube diameter.

References

[1] D. M. Goebel and I. Katz, “Fundamentals of Electric Propulsion: Ion and Hall Thrusters.”

[2] “NASA Technology Roadmaps TA 2: In-Space Propulsion Technologies,” 2015.

[3] E. Y. Choueiri, “A Critical History of Electric Propulsion: The First 50 Years (1906–1956),” *J. Propuls. POWER*, vol. 20, no. 2, pp. 193–203.

[4] J. S. Sovey, V. K. Rawlin, and M. J. Patterson, “Ion Propulsion Development Projects in U.S.: Space Electric Rocket Test I to Deep Space 1,” *J. Propuls. Power*, vol. 17, no. 3, pp. 517–526, 2001.

[5] A. E. Ozturk, E. Turkoz, A. Ozgen, and M. Celik, “Design and thermal analysis of the insert region heater of a lanthanum hexaboride hollow cathode,” *RAST 2013 - Proc. 6th Int. Conf. Recent Adv. Sp. Technol.*, pp. 607–612, 2013.

[6] H. Kamhawi and J. Van Noord, “Development and Testing of High Current Hollow Cathodes for High Power Hall Thrusters,” *AIAA/ASME/SAE/ASEE Jt. Propuls. Conf. Exhib. 35th, Los Angeles, CA, June 20-24, 1999*.

[7] D. J. Warner, R. D. Branam, and W. a. Hargus, “Ignition and Plume Characteristics of Low-Current Cerium and Lanthanum Hexaboride Hollow Cathodes,” *J. Propuls. Power*, vol. 26, no. 1, pp. 130–134, 2010.

[8] L. P. Rand and J. D. Williams, “Instant Start Electride Hollow Cathode,” *33rd Int. Electr. Propuls. Conf.*, pp. 1–11, 2013.

[9] K. R. Trent, M. S. McDonald, R. B. Lobbia, A. D. Gallimore, and H. Cathode, “Time-resolved Langmuir Probing of a New Lanthanum Hexaboride (LaB 6) Hollow Cathode,” *IEPC*, pp. 1–10, 2011.

[10] R. Albertoni, M. Andrenucci, D. Pedrini, and F. Paganucci, “Preliminary Characterization of a LaB6 Hollow Cathode for Low-Power Hall Effect Thrusters,” *33rd Int. Electr. Propuls. Conf.*, pp. 1–8, 2013.

[11] D. M. Goebel and E. Chu, “High-Current Lanthanum Hexaboride Hollow Cathode for High-Power Hall Thrusters,” *48th AiAA/ASME/SAE/ASEE Jt. Propuls. Conf.*, 2012.

[12] A. Sengupta, “Destructive Physical Analysis of Hollow Cathodes from the Deep Space 1 Flight Spare Ion Engine 30,000 Hr Life Test,” *29th Int. Electr. Propuls. Conf. …*, vol. 1, pp. 1–17, 2005.

[13] D. M. Goebel and E. Chu, “High-Current Lanthanum Hexaboride Hollow Cathode for High-Power Hall Thrusters,” *J. Propuls. Power*, vol. 30, no. 1, pp. 35–40, 2014.

[14] P. D. Reader and E. V. Pawlik, “Cathode Durability Tests in Mercury Electron-

bombardment Ion Thrustors," Cleveland, Ohio, 1967.

[15] V. K. Rawlin and W. R. Kerslake, "DURABILITY OF THE SERT ll HOLLOW CATHODE AND FUTURE APPLICATIONS OF HOLLOW CATHODES," in *AIAA 7th Electric Propulsion Conference*, 1969, pp. 1–15.

[16] V. K. Rawlin and E. V. Pawlik, "A Mercury Plasma-Bridge Neutralizer," in *AIAA Electric propulsion and Plasmadynamics conference*, 1967, vol. 5, no. 7, pp. 814–820.

[17] F. Gulczinski and R. Spores, "Analysis of Hall-effect thrusters and ion engines for orbit transfer missions," *Am. Inst. Aeronaut. …*, pp. 1–18, 1996.

[18] M. R. Nakles, W. A. Hargus, J. J. Delgado, and R. L. Corey, "A Performance Comparison of Xenon and Krypton Propellant on an SPT-100 Hall Thruster," *Int. Electr. Propuls. Conf.*, 2011.

[19] A. Kieckhafer and L. B. King, "Energetics of Propellant Options for High-Power Hall Thrusters," *J. Propuls. POWER*, vol. 23, pp. 21–26, 2007.

[20] W. R. Hudson and A. J. Weigand, "HOLLOW CATHODES WITH BaO IMPREGNATED, POROUS TUNGSTEN INSERTS AND TIPS," in *AIAA 10th Electric Propulsion Conference*, 1973, pp. 1–13.

[21] J. M. Lafferty, "Boride Cathodes," *J. Appl. Phys.*, vol. 22, no. 3, pp. 299–309, 1951.

[22] H. E. Gallagher, "Poisoning of LaB6 Cathode," *J. Appl. Phys.*, vol. 40, no. 1, pp. 44–50, 1968.

[23] M. J. Mirtich and W. A. Kerslake, "Long Lifetime Hollow Cathodes for 30-CM Mercury Ion Thrusters," Key Biscayne, 1976.

[24] C. B. Carpenter and M. J. Patterson, "High-Current Hollow Cathode Development," *IEPC 2001*, 2001.

[25] T. R. Verhey and G. S. Macrae, "Requirements for Long-Life Operation of Inert Gas Hollow Cathodes Preliminary Report," in *21st International Electric Propulsion Conference*, 1990, pp. 1–17.

[26] R. E. Thomas, H. Kamhawi, and G. J. Williams, "High Current Hollow Cathode Plasma Plume Measurements," *33rd Int. Electr. Propuls. Conf.*, 2013.

[27] D. Goebel, E. Chu, and Jpl, "High Current Lanthanum Hexaboride Hollow Cathodes for High Power Hall Thrusters," *32nd Int. Electr. Propuls. Conf.*, pp. 1–16, 2011.

[28] D. M. Goebel, A. T. Forrester, and S. Johnston, "La–Mo emitters in hollow cathodes," *Am. Inst. Phys.*, no. 10, pp. 1468–83504, 1980.

[29] D. Asselin, "Characterization of the Near Plume Region of a Low Current Hollow Cathode," 2011.

[30] R. B. Lobbia and B. E. Beal, "Recommended Practice for Use of Langmuir Probes in Electric Propulsion Testing," *J. Propuls. Power*, vol. 33, no. 3, pp. 566–581, 2017.

[31] B. Rubin and J. D. Williams, “HOLLOW CATHODE CONDITIONING AND DISCHARGE INITIATION STUDIES *.”

Appendix A

Telemetry Data

Table 6 - LaB_6 telemetry data

LaB_6			
m	**I_kpr**	**V_discharge**	**Vpk2pk**
sccm	A	V	V
Discharge current of 4A			
6	1.5	49.99	4
6	1	43.4	35
6	0.5	42.3	12
4	1.5	57	97
4	1	39.8	95
4	0.5	62.4	166
2	1.5	39.8	5
Discharge current of 3A			
6	1.5	42.9	9
6	1	43	13
6	0.5	45.6	15
4	1.5	67.7	79
4	1	42.2	18
4	0.5	46.6	14
2	1.5	39.3	30
Discharge current of 2A			
6	1.5	39.4	10
6	1	46.6	15
LaB_6			
6	0.5	48.3	13
4	1.5	29.6	22
4	1	42.6	17
4	0.5	46.9	14
2	1.5	42.3	36
Discharge current of 1A			
6	1.5	31.6	7
6	1	46.6	19
6	0.5	54.6	13
4	1.5	48.8	24
4	1	42.9	18

4	0.5	55.9	13
2	1.5	64.3	34
Discharge current of 0A			
6	1.5	24.9	10
6	1	34	22
6	0.5	32.2	14
4	1.5	68.5	25
4	1	27.6	21
4	0.5	40.7	22

Table 7 - BaO telemetry data

BaO			
m	**I_kpr**	**V_discharge**	**Vpk2pk**
sccm	A	V	V
Discharge current of 4A			
6	1.5	34.1	36
6	1	41	26
6	0.5	39.4	28
4	1.5	34.6	44
4	1	37.3	42
Discharge current of 3A			
6	1.5	35.6	24
6	1	41	26
6	0.5	42.6	18
4	1.5	34.6	44
4	1	37.3	42
Discharge current of 2A			
6	1.5	48.9	56
6	1	50.4	48
6	0.5	46.2	18
4	1.5	33	34
4	1	37.3	36
2	1.5	38.6	40
2	1	43.2	34
Discharge current of 1A			
6	1.5	27.8	16
6	1	48.1	18
6	0.5	48.2	22
4	1.5	30.8	30
4	1	37	26

2	1.5	35.6	32
2	1	47.2	28
2	0.5	54.4	30
Discharge current of 0A			
6	1.5	7.4	16
6	1	21.8	34
6	0.5	58	42
4	1.5	9.3	44
4	1	19.9	75
2	1.5	7.9	26
2	1	17.3	24

Table 8 - Cermet telemetry data

Cermet			
m	**I_kpr**	**V_anode**	**Vpk2pk**
sccm	A	V	V
Anode current of 4A			
6	1.5	47.1	19
6	1	48.1	29
6	0.5	42.3	22
4	1.5	68.7	21
4	1	66.3	84
Anode current of 3A			
6	1.5	43.7	21
6	1	45.3	14
6	0.5	41.9	27
4	1.5	47.9	18
4	1	46	21
Anode current of 2A			
6	1.5	37.9	21
6	1	47.4	21
6	0.5	44.9	22
4	1.5	47.5	32
4	1	53.4	31
Anode current of 1A			
6	1.5	46.4	18
6	1	52.3	21
6	0.5	48.8	24
4	1.5	53.8	27

4	1	53.4	31
Anode current of 0A			
6	1.5	23.9	16
6	1	36.2	23
6	0.5	35.5	12
4	1.5	17.4	45
4	1	20.6	18

IVm Maps

Lab6

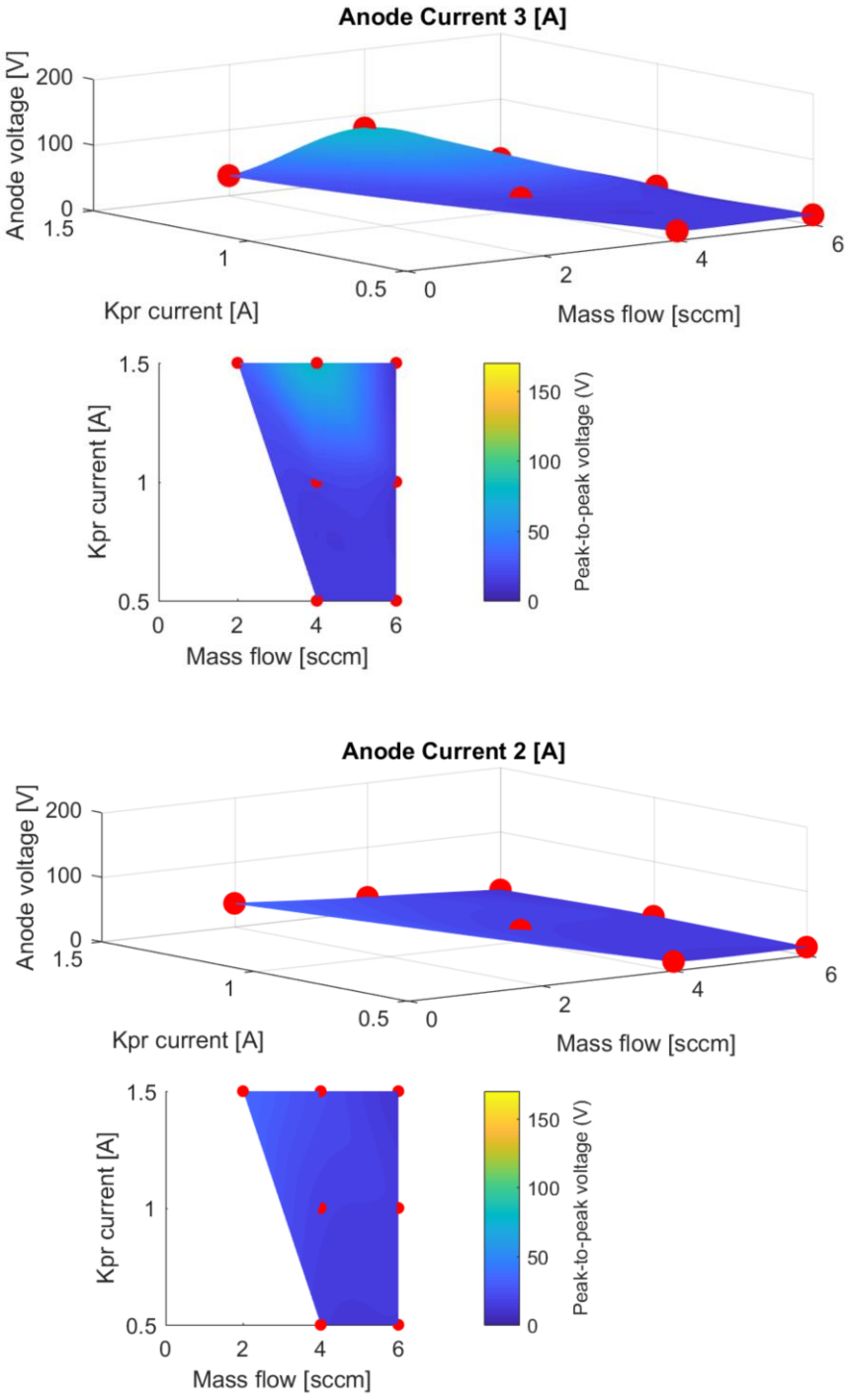

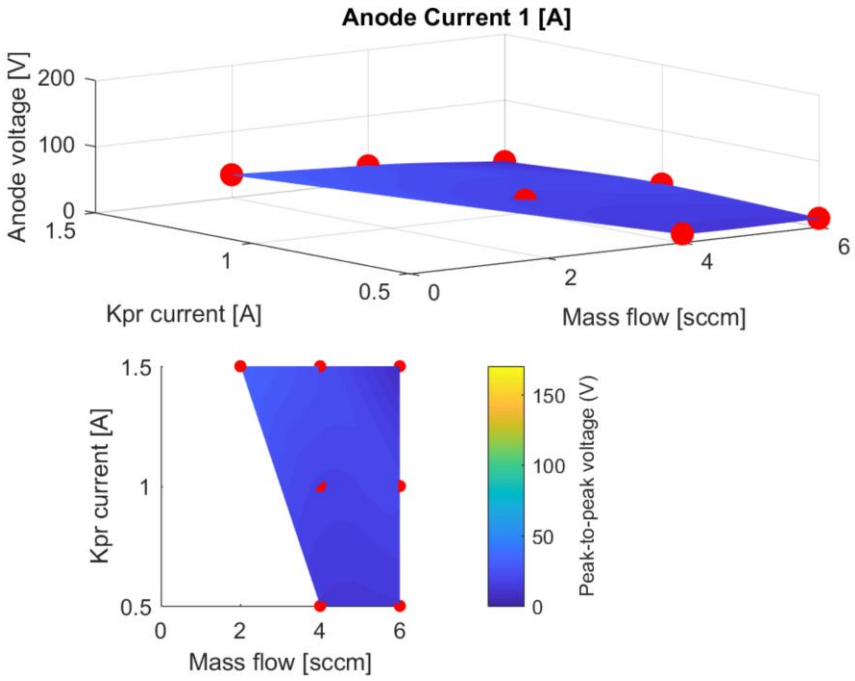
Anode Current 1 [A]
Anode voltage [V]
200
100
0
1.5
1
0.5
Kpr current [A]
0
2
4
6
Mass flow [sccm]
Kpr current [A]
1.5
1
0.5
0
2
4
6
Mass flow [sccm]
150
100
50
0
Peak-to-peak voltage (V)

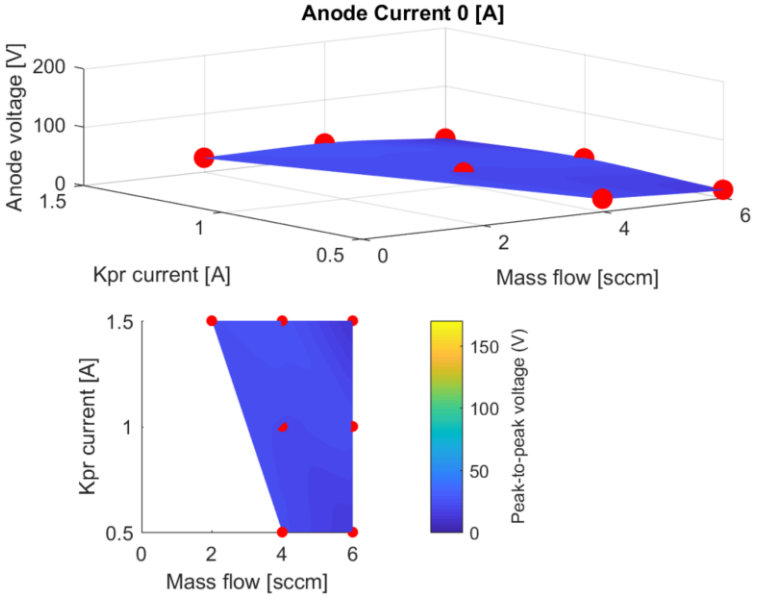
Anode Current 0 [A]
Anode voltage [V]
200
100
0
1.5
1
0.5
Kpr current [A]
0
2
4
6
Mass flow [sccm]
Kpr current [A]
1.5
1
0.5
0
2
4
6
Mass flow [sccm]
150
100
50
0
Peak-to-peak voltage (V)

BaO

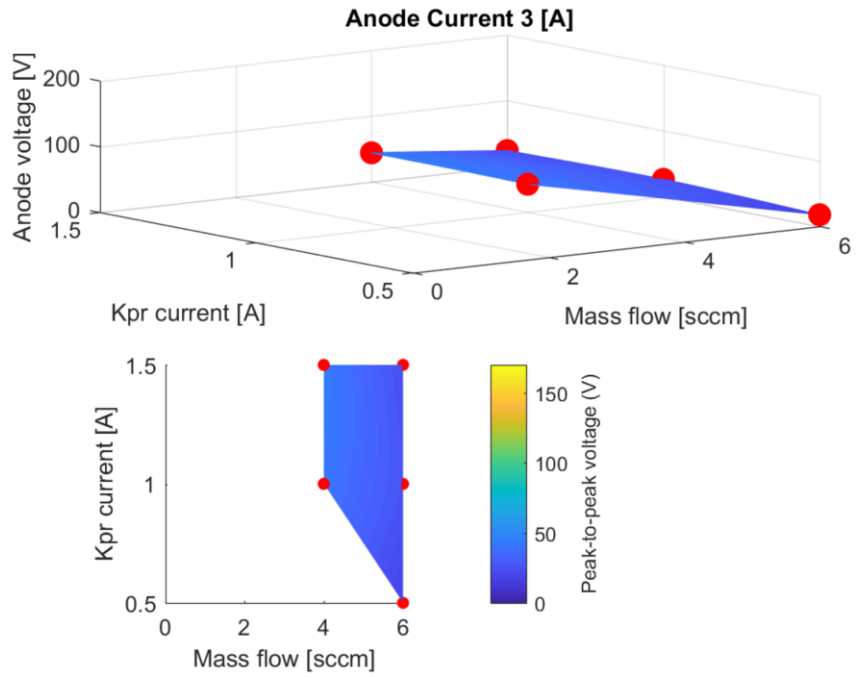
Anode Current 3 [A]
Anode voltage [V]
200
100
0
1.5
1
0.5
Kpr current [A]
0
2
4
6
Mass flow [sccm]
Kpr current [A]
1.5
1
0.5
0
2
4
6
Mass flow [sccm]
150
100
50
0
Peak-to-peak voltage (V)

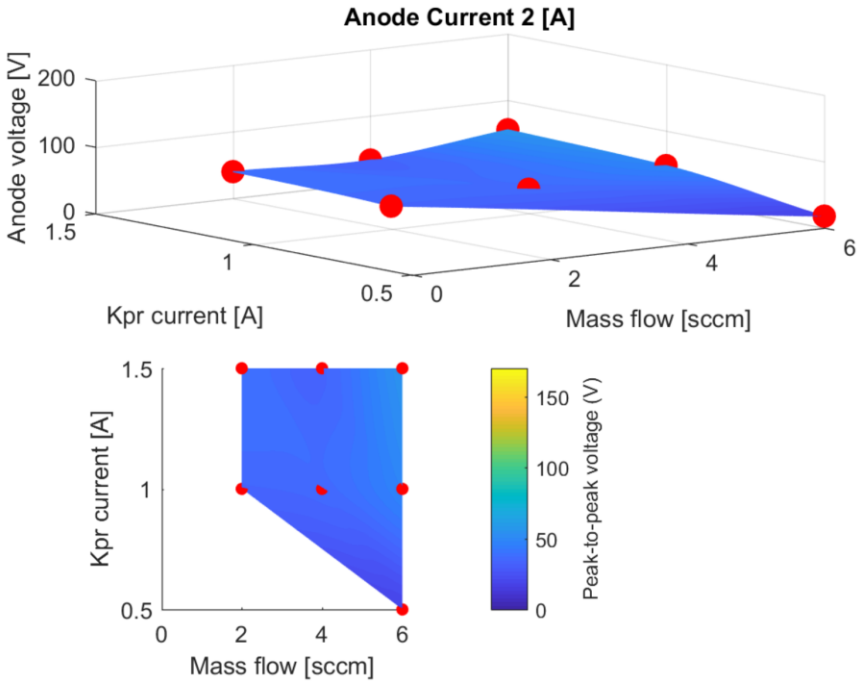
Anode Current 2 [A]
Anode voltage [V]
200
100
0
1.5
1
0.5
Kpr current [A]
0
2
4
6
Mass flow [sccm]
Kpr current [A]
1.5
1
0.5
0
2
4
6
Mass flow [sccm]
150
100
50
0
Peak-to-peak voltage (V)

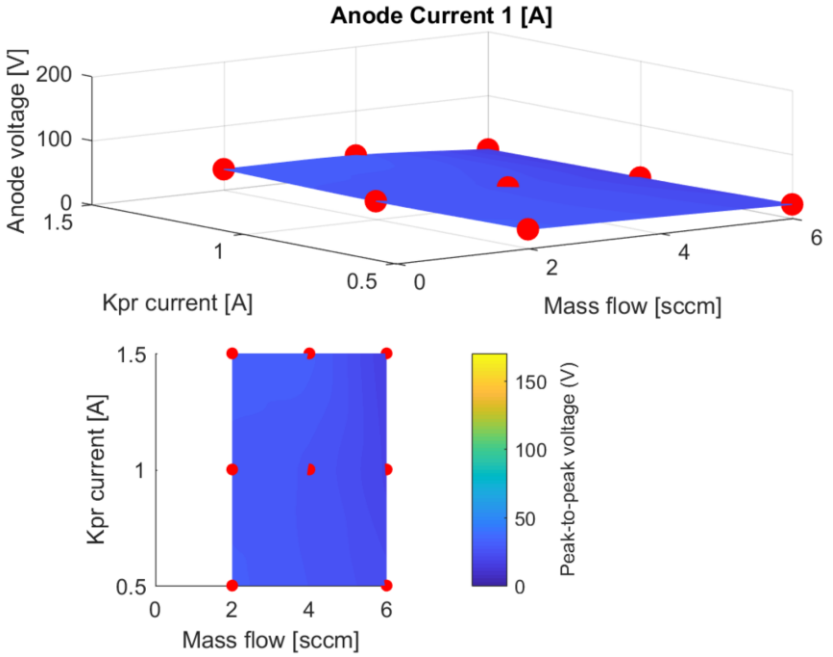
Anode Current 1 [A]
Anode voltage [V]
200
100
0
1.5
1
0.5
Kpr current [A]
0
2
4
6
Mass flow [sccm]
Kpr current [A]
1.5
1
0.5
0
2
4
6
Mass flow [sccm]
150
100
50
0
Peak-to-peak voltage (V)

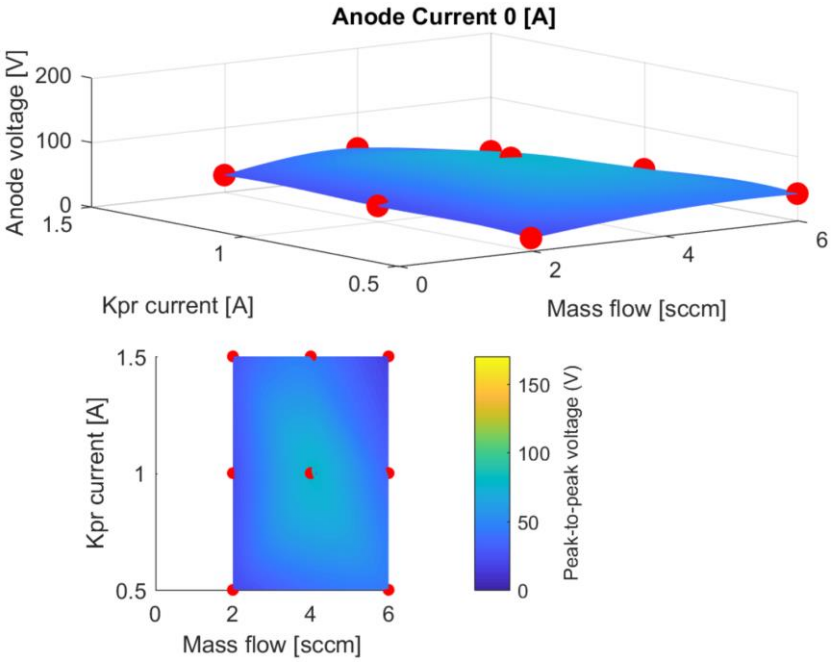
Anode Current 0 [A]
Anode voltage [V]
200
100
0
1.5
1
0.5
Kpr current [A]
0
2
4
6
Mass flow [sccm]
Kpr current [A]
1.5
1
0.5
0
2
4
6
Mass flow [sccm]
150
100
50
0
Peak-to-peak voltage (V)

Cermet

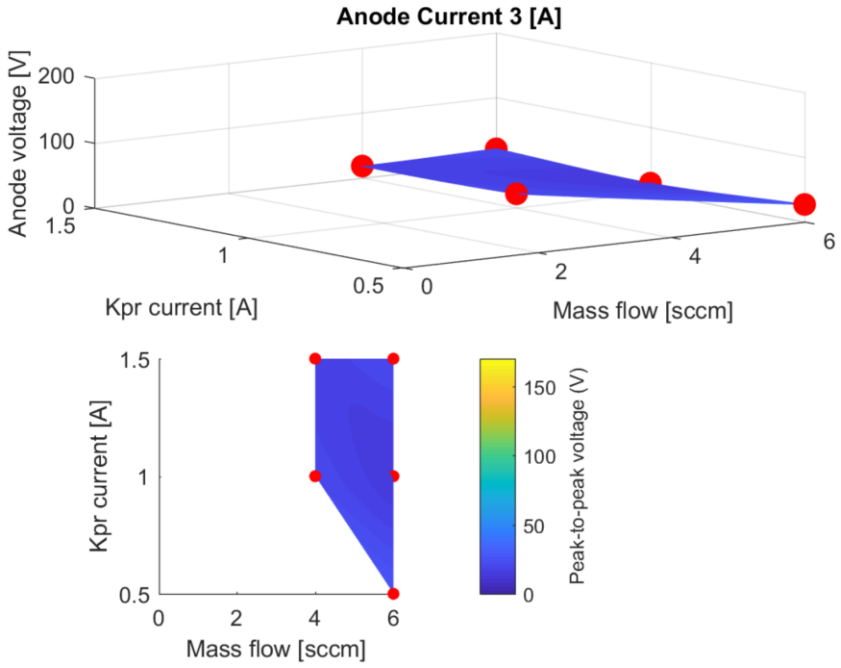
Anode Current 3 [A]
Anode voltage [V]
200
100
0
1.5
1
0.5
Kpr current [A]
0
2
4
6
Mass flow [sccm]
1.5
1
0.5
Kpr current [A]
0
2
4
6
Mass flow [sccm]
150
100
50
0
Peak-to-peak voltage (V)

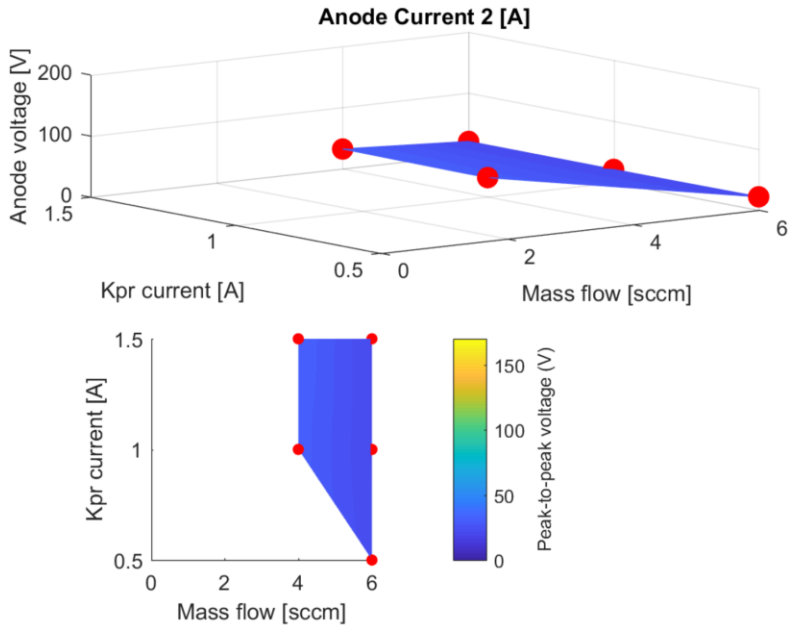
Anode Current 2 [A]
Anode voltage [V]
200
100
0
1.5
1
0.5
Kpr current [A]
0
2
4
6
Mass flow [sccm]
1.5
1
0.5
Kpr current [A]
0
2
4
6
Mass flow [sccm]
150
100
50
0
Peak-to-peak voltage (V)

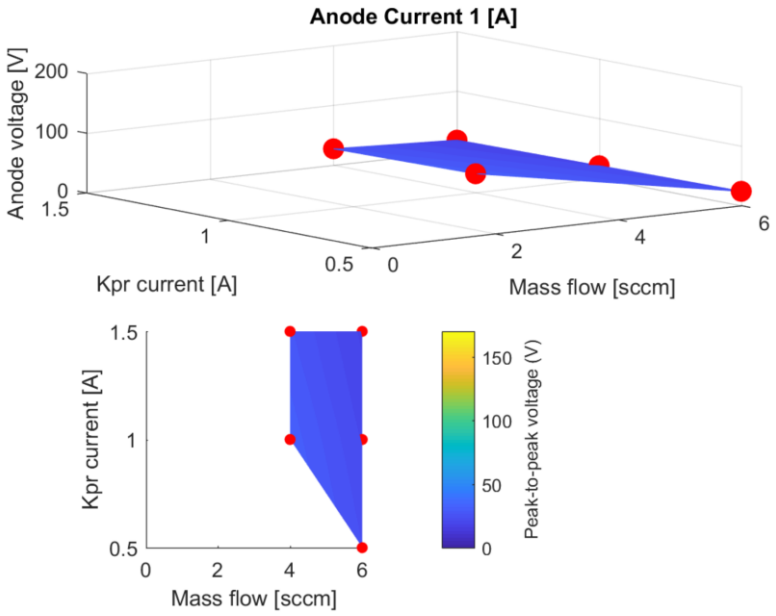
Anode Current 1 [A]
Anode voltage [V]
200
100
0
1.5
1
0.5
Kpr current [A]
0
2
4
6
Mass flow [sccm]
1.5
1
0.5
Kpr current [A]
0
2
4
6
Mass flow [sccm]
150
100
50
0
Peak-to-peak voltage (V)

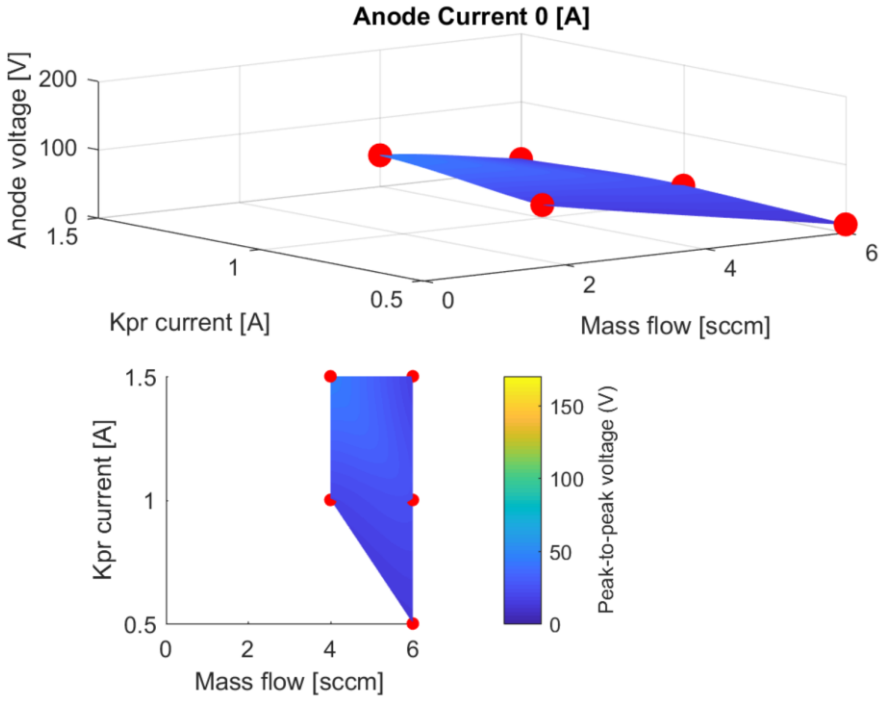
Anode Current 0 [A]
Anode voltage [V]
200
100
0
1.5
1
0.5
Kpr current [A]
0
2
4
6
Mass flow [sccm]
1.5
1
0.5
Kpr current [A]
0
2
4
6
Mass flow [sccm]
150
100
50
0
Peak-to-peak voltage (V)

Appendix B

LaB_6

	6 sccm, 1.5 A-kpr, and 4 A-An			6 sccm, 1.0 A-kpr, and 4 A-An		
Position	Te	n	Vp	Te	n	Vp
40	5.0	4.8E+15	35.0	1.9	1.1E+14	20.0
38	4.9	5.3E+15	35.0	1.9	1.2E+14	20.0
36	4.9	5.7E+15	35.0	1.9	1.3E+14	20.0
34	4.9	6.3E+15	35.0	1.9	1.5E+14	20.0
32	4.9	6.9E+15	35.0	1.9	1.8E+14	20.0
30	4.9	7.6E+15	35.0	2.0	2.2E+14	20.0
28	4.9	8.5E+15	35.0	2.0	2.8E+14	20.0
26	4.9	9.6E+15	35.0	2.1	3.6E+14	20.0
24	5.0	1.1E+16	35.0	2.2	5.0E+14	20.0
22	5.0	1.3E+16	35.0	--	--	--
20	5.1	1.5E+16	35.0	--	--	--
18	5.1	1.9E+16	35.0	--	--	--
16	5.2	2.4E+16	35.0	--	--	--
14	5.4	3.0E+16	35.0	--	--	--
12	5.5	4.0E+16	35.0	--	--	--
10	5.3	5.8E+16	35.0	--	--	--

Cermet

	6 sccm, 1.5 A-kpr, 4 A-An			6 sccm, 1 A-kpr, 4 A-An			6 sccm 1.5 A-kpr, 2 A-An			6 sccm, 1 A-kpr, 2 A-An		
Position	Te	n	Vp	Te	n	Vp	Te	n	Vp	Te	n	Vp
40	7.6	8.0E+15	51.8	7.2	6.9E+15	48.6	4.6	4.4E+15	38.9	5.0	2.3E+15	37.9
38	7.6	8.6E+15	51.8	7.5	8.8E+15	51.8	4.0	4.1E+15	35.7	5.8	4.1E+15	43.9
36	7.2	7.9E+15	48.6	7.6	9.5E+15	51.8	4.5	5.7E+15	38.9	6.0	5.0E+15	45.5
34	7.6	1.0E+16	51.8	7.8	1.1E+16	53.4	4.0	5.3E+15	35.7	6.3	6.2E+15	47.0
32	7.5	1.0E+16	50.2	7.3	9.4E+15	48.6	4.5	7.2E+15	38.9	5.7	6.5E+15	43.9
30	8.2	1.4E+16	55.0	8.2	1.4E+16	55.0	3.1	3.6E+15	29.2	5.0	6.5E+15	40.9
28	8.4	1.5E+16	55.0	7.9	1.3E+16	51.8	3.1	4.2E+15	29.2	5.5	8.6E+15	43.9
26	7.8	1.4E+16	50.2	8.0	1.5E+16	51.8	3.1	4.9E+15	29.2	5.2	9.2E+15	42.4
24	8.4	1.8E+16	53.4	9.3	2.2E+16	58.3	3.1	4.1E+15	27.6	3.4	4.4E+15	30.3
22	7.8	1.7E+16	48.6	10.3	2.7E+16	61.5	3.2	6.7E+15	29.2	5.3	7.3E+15	39.4
20	8.2	2.4E+16	51.8	9.8	3.1E+16	59.9	3.2	5.9E+15	27.6	6.7	1.4E+16	48.5
18	8.1	2.7E+16	50.2	10.5	3.9E+16	61.5	3.2	7.4E+15	27.6	7.0	1.8E+16	50.0
16	8.1	3.2E+16	48.6	10.6	4.5E+16	59.9	3.4	9.0E+15	27.6	7.7	2.4E+16	53.0
14	7.3	3.8E+16	45.4	4.8	2.8E+16	34.0	3.4	1.2E+16	27.6	4.1	1.3E+16	33.3
12	5.5	3.7E+16	35.7	3.8	2.6E+16	27.6	3.5	2.2E+16	29.2	4.1	2.0E+16	33.3
10	4.1	3.4E+16	27.6	3.5	3.7E+16	26.0	3.5	2.9E+16	29.2	3.6	2.3E+16	30.3

BaO

	6 sccm, 1.5 A-kpr, and 4 A-An			6 sccm, 1.0 A-kpr, and 4 A-An			6 sccm, 1.5 A-kpr, and 2 A-An			4 sccm, 1 A-kpr, and 4 A-An			2 sccm, 1.5 A-kpr, and 4 A-An			2 sccm, 1.5 A-kpr, 2 A-An		
Position	Te	n	Vp	Te	n	Vp	Te	n	Vp	Te	n	Vp	Te	n	Vp	Te	n	Vp
40	3.4	6.7E+15	24.2	3.5	5.2E+15	23.7	5.2	2.4E+15	37.3	4.2	4.9E+15	26.8	3.7	6.1E+15	25.6	3.0	3.4E+15	28.8
38	3.4	7.4E+15	24.2	3.4	5.2E+15	22.7	5.2	2.6E+15	37.3	4.1	5.8E+15	26.8	3.7	6.4E+15	25.6	3.0	3.6E+15	28.8
36	3.3	6.0E+15	22.7	3.4	5.7E+15	22.7	5.2	2.9E+15	37.3	4.2	5.9E+15	26.8	3.8	6.8E+15	25.6	3.0	3.9E+15	28.8
34	3.4	6.6E+15	22.7	3.5	7.4E+15	23.7	5.2	3.1E+15	37.3	4.2	6.3E+15	26.8	3.8	7.2E+15	25.6	3.0	4.3E+15	28.8
32	3.4	7.9E+15	22.7	3.6	6.6E+15	23.7	5.1	3.5E+15	37.3	4.5	5.6E+15	26.8	3.8	9.9E+15	26.7	3.0	4.6E+15	28.8
30	3.5	7.4E+15	22.7	3.7	8.8E+15	24.7	5.1	4.1E+15	37.3	4.5	6.2E+15	26.8	3.9	1.1E+16	26.7	3.0	5.1E+15	28.8
28	3.8	1.0E+16	24.2	3.7	9.8E+15	24.7	5.1	4.7E+15	37.3	4.6	6.9E+15	26.8	4.0	8.9E+15	25.6	3.0	5.7E+15	28.8
26	3.5	9.6E+15	22.7	3.7	9.0E+15	23.7	5.1	5.4E+15	37.3	4.6	8.4E+15	26.8	4.1	1.2E+16	26.7	3.1	6.3E+15	28.8
24	5.6	1.9E+16	31.8	3.8	1.1E+16	23.7	4.9	6.1E+15	36.1	4.5	1.0E+16	26.8	4.2	1.4E+16	26.7	3.3	6.9E+15	28.8
22	3.4	1.5E+16	22.7	3.8	1.6E+16	24.7	4.7	7.7E+15	36.1	4.5	1.2E+16	26.8	4.3	1.5E+16	26.7	3.4	7.8E+15	28.8
20	3.5	2.0E+16	22.7	3.8	1.7E+16	24.7	4.4	8.4E+15	33.6	4.7	1.4E+16	26.8	4.4	1.7E+16	26.7	3.5	8.9E+15	28.8
18	3.5	2.4E+16	22.7	3.9	1.9E+16	24.7	4.2	1.0E+16	32.4	4.7	1.6E+16	26.8	4.6	1.8E+16	26.7	3.6	1.0E+16	28.8
16	3.5	2.8E+16	22.7	3.8	2.5E+16	24.7	4.1	1.5E+16	32.4	4.8	2.0E+16	26.8	4.8	2.1E+16	26.7	4.0	1.2E+16	28.8
14	3.5	3.8E+16	22.7	3.8	3.6E+16	24.7	4.1	1.9E+16	32.4	4.7	3.2E+16	27.8	5.0	2.4E+16	26.7	4.1	1.4E+16	28.8
12	3.4	5.1E+16	22.7	3.8	4.3E+16	24.7	4.1	2.6E+16	32.4	4.7	4.0E+16	27.8	5.2	3.6E+16	27.8	4.5	1.8E+16	28.8
10	3.3	7.9E+16	22.7	4.8	6.7E+16	28.8	4.1	3.4E+16	32.4	4.8	5.2E+16	27.8	5.4	4.5E+16	27.8	4.6	2.4E+16	28.8